

1 **Title: Inheritance of old mitochondria controls early CD8<sup>+</sup> T cell fate commitment and is**  
2 **regulated by autophagy**

3 Mariana Borsa<sup>1,5,6</sup>, Ana Victoria Lechuga-Vieco<sup>1</sup>, Amir H. Kayvanjoo<sup>4</sup>, Yavuz Yazicioglu<sup>1</sup>, Ewoud B.  
4 Compeer<sup>1</sup>, Felix C. Richter<sup>1</sup>, Hien Bui<sup>2</sup>, Michael L. Dustin<sup>1</sup>, Pekka Katajisto<sup>2,3</sup>, Anna Katharina Simon<sup>1,5</sup>

5 <sup>1</sup>Kennedy Institute of Rheumatology, University of Oxford, Oxford, England;

6 <sup>2</sup>HiLife, Institute of Biotechnology, University of Helsinki, Helsinki, Finland;

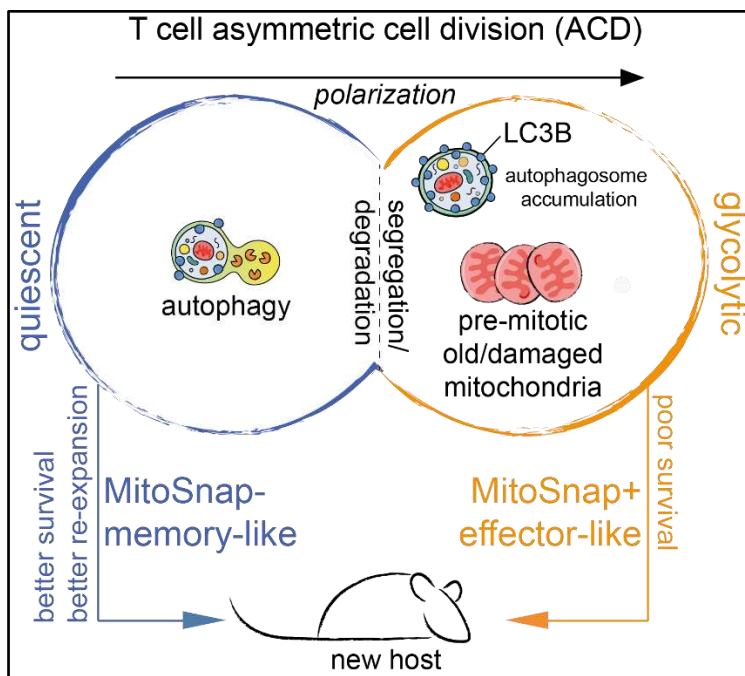
7 <sup>3</sup>Department of Cell and Molecular Biology (CMB), Karolinska Institute, Stockholm, Sweden;

8 <sup>4</sup>Max-Delbrück-Center for Molecular Medicine, Berlin, Germany

9 <sup>5</sup>Corresponding author: mariana.borsa@kennedy.ox.ac.uk; katja.simon@mdc-berlin.de

10 <sup>6</sup>Lead contact

11



12

13 The MitoSnap model allows tracking of pre-mitotic and post-mitotic cell cargoes.

14

15 Both segregation and degradation (autophagy) contribute to the asymmetric inheritance of old mitochondria.

16

Old mitochondria impact cell metabolism and function.

17

Cells devoid of old mitochondria exhibit better memory potential *in vivo*.

18

19 **Abstract**

20 T cell immunity is impaired during ageing, particularly in memory responses needed for efficient  
21 vaccination. Autophagy and asymmetric cell division (ACD) are cell biological mechanisms key to  
22 memory formation, which undergo a decline upon ageing. However, despite the fundamental  
23 importance of these processes in cellular function, the link between ACD and *in vivo* fate decisions has  
24 remained highly correlative in T cells and in the field of mammalian ACD overall. Here we provide robust  
25 causal evidence linking ACD to *in vivo* T cell fate decisions and our data are consistent with the concept  
26 that initiation of asymmetric T cell fates is regulated by autophagy. Analysing the proteome of first-  
27 daughter CD8<sup>+</sup> T cells following TCR-triggered activation, we reveal that mitochondrial proteins rely on  
28 autophagy for their asymmetric inheritance and that damaged mitochondria are polarized upon first  
29 division. These results led us to evaluate whether mitochondria were asymmetrically inherited and to  
30 functionally address their impact on T cell fate. For this we used a novel mouse model that allows  
31 sequential tagging of mitochondria in mother and daughter cells, enabling their isolation and subsequent  
32 *in vivo* analysis of CD8<sup>+</sup> T cell progenies based on pre-mitotic cell cargo. Autophagy-deficient CD8<sup>+</sup> T  
33 cells showed impaired clearance and symmetric inheritance of old mitochondria, suggesting that  
34 degradation events promote asymmetry and are needed to generate T cells devoid of old organelles.  
35 Daughter cells inheriting old mitochondria are more glycolytic and upon adoptive transfer show reduced  
36 memory potential, whereas daughter cells that have not inherited old mitochondria from the mother cell  
37 are long-lived and expand upon cognate-antigen challenge. Proteomic and single-cell transcriptomic  
38 analysis of cells inheriting aged mitochondria suggest that their early fate divergence relies on one  
39 carbon metabolism as a consequence of poor mitochondrial quality and function. These findings  
40 increase our understanding of how T cell diversity is early-imprinted during division and will help foster  
41 the development of strategies to modulate T cell function.

42

## 43 Introduction

44 Efficient immune responses rely on the coordinated function of different immune cell types, which also  
45 requires generation of diversity within the same cell type. In the context of CD8<sup>+</sup> T cells, one single cell  
46 is able to differentiate and generate progeny with heterogeneous fates upon activation<sup>1,2</sup>. Activation of  
47 a naïve T cell by its cognate antigenic epitope leads to the differentiation of short-lived effector cells that  
48 exert cytotoxic effector functions, and long-lived memory cells that self-renew and differentiate upon  
49 antigenic re-challenge and are central to vaccination efficacy. Despite increased understanding of  
50 mechanisms that contribute to fate decision during CD8<sup>+</sup> T cell differentiation, there is still no consensus  
51 on when these decisions are made, and particularly how long-lived memory T cells are formed<sup>3-5</sup>.  
52 Moreover, during aging T cell memory is severely impaired<sup>6,7</sup>, and senescent CD8<sup>+</sup> T cell subsets that  
53 exhibit DNA damage, cell cycle arrest, mitochondrial dysfunction due to defective mitophagy<sup>8</sup>, and  
54 global poor effector function accumulate<sup>9-11</sup>. Amongst the cellular processes that benefit the formation  
55 and maintenance of memory CD8<sup>+</sup> T cells but which are negatively impacted by ageing<sup>6,12,13</sup>, there are  
56 two highly conserved mechanisms: macroautophagy (hereafter termed autophagy) and asymmetric cell  
57 division (ACD).

58 Autophagy involves the recycling and degradation of cellular cargoes, which occurs via the engulfment  
59 of cellular components by double-membrane structures called autophagosomes, and their delivery to  
60 lysosomes for degradation. The regulation by autophagy of immune cell fate decision is cell- and  
61 context-dependent<sup>14</sup>. In CD8<sup>+</sup> T cell differentiation, autophagy loss results in an impaired memory  
62 response<sup>6,15,16</sup>, which is at least partly caused by accumulation of damaged organelles<sup>17,18</sup>.

63 ACD has been well characterised in model organisms such as yeast, *Drosophila melanogaster* and  
64 *Caenorhabditis elegans*<sup>19</sup>, but evidence of the impact of this mechanism on cell fate in mammalian cells  
65 remains correlative and inconclusive<sup>20</sup>. In cells from the haematopoietic lineage, this is a consequence  
66 of technical limitations as *in vivo* functional readouts of sibling cells have relied on cell cargoes that do  
67 not directly influence fate decisions and/or show dynamic and variable expression. Thus, a critical  
68 question remains: is inherited material synthesized post-cell division, or is it inherited asymmetrically?  
69 Here we address this question using CD8<sup>+</sup> T cells. ACD in CD8<sup>+</sup> T cells is important for the generation  
70 of two distinct cell types, through the early generation of effector-like and memory-like daughter cells<sup>21</sup>  
71 that occurs from the first mitosis after naïve T cell activation by high-affinity TCR stimulation<sup>22,23</sup>. The  
72 daughter cells emerging from ACD inherit several layers of asymmetry, including the differential  
73 expression of surface markers, transcription factors, divergent metabolic activity and translation<sup>24-27</sup>.  
74 However, a direct link between asymmetric inheritance of pre-mitotic T cell cargo and the future fate of  
75 emerging daughter cells *in vivo* has not been made. Thus, solid causal evidence linking ACD to fate  
76 decisions is lacking in T cells and in the field of mammalian ACD in general.

77 Because it is unclear whether cell cargo degradation can contribute to cell division asymmetries, we  
78 performed an integrated functional analysis of the contribution of autophagy and ACD to CD8<sup>+</sup> T cell  
79 differentiation. We identified damaged mitochondria as asymmetrically inherited cargo, and this  
80 asymmetry is further deepened on mitophagy. Then, using a novel mouse model that allows specific  
81 labelling of mitochondria before and after cell division, we tracked mitochondrial inheritance and  
82 biogenesis, ensuring that this cell cargo was not perturbed by post-mitotic changes in CD8<sup>+</sup> T cell  
83 progenies. This novel tool allowed us to follow the presence of pre-mitotic mitochondria by imaging and  
84 flow cytometry, and evaluate the impact of mitochondrial inheritance by proteomics, scRNAseq and *in*  
85 *vivo* transfer of daughter cells. Our results suggest that autophagy contributes to the generation of early  
86 divergent cell fates by promoting both clearance and asymmetric partitioning of old mitochondria.  
87 Furthermore, we are the first to unequivocally draw a causal link between the inheritance of cell cargo  
88 to future fate commitment, as old mitochondria caused poor memory potential in CD8<sup>+</sup> T cell immune  
89 responses. Our findings offer new insight into how T cell diversity is imprinted early during cell division,  
90 and how organelle ageing regulates CD8<sup>+</sup> T cell metabolism and function, facilitating more refined  
91 therapeutic approaches to T cell modulation.

92

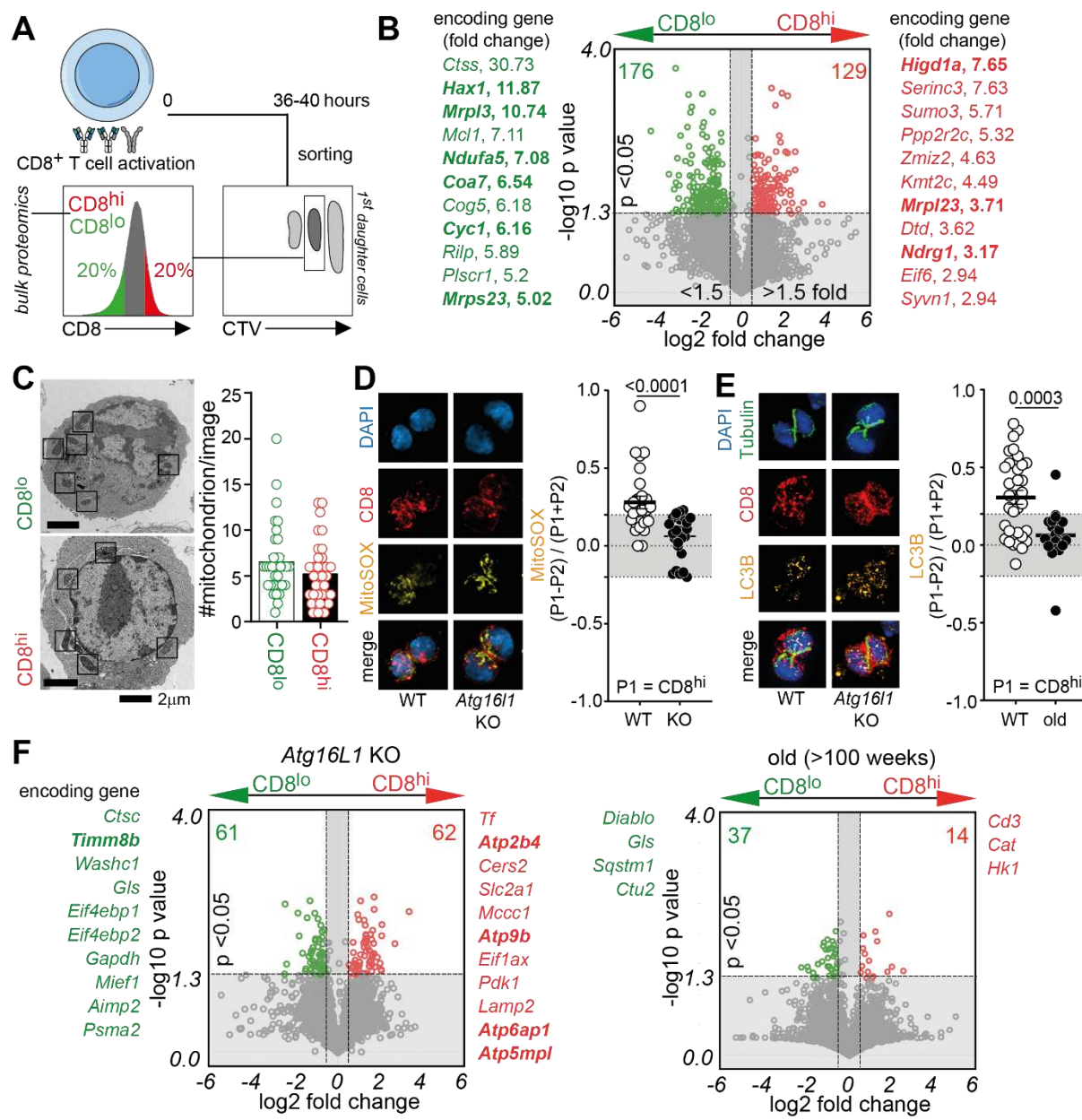
## 93 Results

94 Divergent proteome and mitochondrial inheritance in CD8<sup>+</sup> T cell mitosis relies on autophagy

95 Asymmetric cell division in CD8<sup>+</sup> T cells results in the unequal inheritance of different cell cargoes that  
96 culminates in divergent transcriptomes between daughter cells<sup>27-30</sup>. We aimed to broaden our

97 understanding of early events of asymmetric segregation by assessing the global proteome of first-  
98 daughter CD8<sup>+</sup> T cells. To that end, we used CD8 as a surrogate marker to classify effector-like (CD8<sup>hi</sup>)  
99 and memory-like (CD8<sup>lo</sup>) progenies. Briefly, we isolated naïve CD8<sup>+</sup> T cells from spleens and lymph  
100 nodes of wild-type (WT) C57BL/6 mice, labelled them with a cell trace dye and activated these cells for  
101 36-40 h on anti-CD3, anti-CD28 and Fc-ICAM-1 coated wells. First-daughter CD8<sup>+</sup> T cells were sorted  
102 into CD8<sup>hi</sup> or CD8<sup>lo</sup> populations as previously described<sup>28</sup> (Fig.1A). Cells were washed and pellets were  
103 used for quantitative label-free high-resolution mass spectrometry. >6000 proteins were identified and  
104 the proteomic ruler method was used to calculate both protein mass and copy numbers of each protein  
105 per cell<sup>31</sup>. We did not observe differences in total protein mass between CD8<sup>hi</sup> and CD8<sup>lo</sup> daughter cells  
106 (Fig. S1A). However, we identified several proteins that were enriched in one of these two populations,  
107 as represented by fold-change in protein copy number between effector-like and memory-like cells  
108 following first mitosis (Fig. 1B). Amongst the top 50 identified targets in each group, we found several  
109 proteins with a role linked to cell metabolism, mitochondrial function and biogenesis, which are  
110 highlighted in bold. Because mitochondria are known to contribute to T cell fate<sup>32,33</sup>, we decided to  
111 focus on these organelles. We aimed to validate the results obtained from this unbiased approach by  
112 imaging mitochondria in mitotic cells and emerging siblings. By electron microscopy, we could neither  
113 observe any differences in mitochondrial content (Fig. 1C), nor any differences in mitochondrial  
114 architecture. The inheritance of mitochondria by daughter cells during mitosis has been superficially  
115 investigated with conflicting results<sup>25,26,34</sup>. Thus, we evaluated whether mitochondrial fitness is different  
116 between CD8<sup>+</sup> T cell siblings. Using the cell permeable probe MitoSOX, we imaged mitochondria  
117 producing high levels of reactive oxygen species (ROS, a readout of damaged organelles), and  
118 observed that CD8<sup>hi</sup> (effector-like) daughter cells had a higher abundance of mitochondrial ROS  
119 production (Fig. 1D). Because damaged mitochondria are targets of autophagy - a mechanism known  
120 to benefit memory CD8<sup>+</sup> T cells - and known to undergo an age-related decline, we interrogated whether  
121 mitophagy contributes to this unequal distribution and quantified MitoSOX inheritance in autophagy-  
122 deficient CD8<sup>+</sup> T cells. Using non-inducible autophagy-deleted CD8<sup>+</sup> T cells (*Atg7<sup>fl/fl</sup> Cd4<sup>Cre</sup>*), we  
123 observed that the immune synapse (IS) area and TCR clustering were distinct between the autophagy-  
124 sufficient and -deficient CD8<sup>+</sup> T cells (Fig. S1B). As it has been described that IS formation and TCR-  
125 affinity and signalling strength are crucial for asymmetric T cell division<sup>21-23</sup>, we excluded that any  
126 differences in T cell activation due to loss of Atg7 interferes with ACD readouts by using an inducible  
127 model of autophagy deletion (*Atg16<sup>fl/fl</sup> Ert2<sup>Cre</sup>*). Here activation happens with functional autophagy, as  
128 *Atg16<sup>fl</sup>* is deleted only upon *in vitro* Z-4-Hydroxytamoxifen (4OHT) treatment (Fig. S1C), and Cre-  
129 recombination events do not result in immediate ATG16L1 loss. We analyzed mitotic CD8<sup>+</sup> T cells by  
130 confocal microscopy at 36-40 h post-activation, and found that autophagy loss abolishes the  
131 asymmetric inheritance of damaged (MitoSOX+) mitochondria (Fig. 1D). To evaluate whether the  
132 autophagic machinery itself is polarized during cell division, we evaluated the expression of the  
133 autophagy-marker LC3B. LC3B is the lipidated and membrane-bound version of Microtubule-  
134 associated protein 1A/1B-light chain 3 (LC3), which functions in autophagy substrate selection and  
135 autophagosome biogenesis and is a target of degradation itself during the autophagic process when no  
136 lysosomal inhibitor is added<sup>14</sup>. As observed for MitoSOX, LC3B was co-inherited by CD8<sup>hi</sup> (effector-like)  
137 daughter cells, suggesting that this daughter cell performs less autophagy/mitophagy, which leads to  
138 the accumulation of autophagy targets. To confirm this, we also evaluated the inheritance of LC3B in  
139 CD8<sup>+</sup> T cells from aged mice, known to show poor ACD potential and low autophagy levels<sup>12,15,16</sup>. We  
140 found that ageing leads to the symmetric inheritance of LC3B (Fig. 1E). Finally, these results could be  
141 correlated with the proteome of CD8<sup>hi</sup> and CD8<sup>lo</sup> daughter cells generated from autophagy-deficient  
142 (inducible *Atg16<sup>fl</sup>* deletion) and aged cells (Fig. 1F), since: i) the numbers of differentially inherited  
143 proteins were lower than the ones observed in WT cells (Fig 1B), and ii) we found fewer and different  
144 proteins linked to mitochondrial function amongst the differentially-inherited in autophagy-deficient and  
145 aged CD8<sup>+</sup> T cells. Together these findings highlight the relevance of autophagy in the establishment  
146 of asymmetric inheritance patterns. Interestingly, the pool of enriched proteins found in CD8<sup>hi</sup> and CD8<sup>lo</sup>  
147 daughter cells was very small in old mice and no mitochondrial proteins were found, perhaps because  
148 both ACD and autophagy decline with age.

149



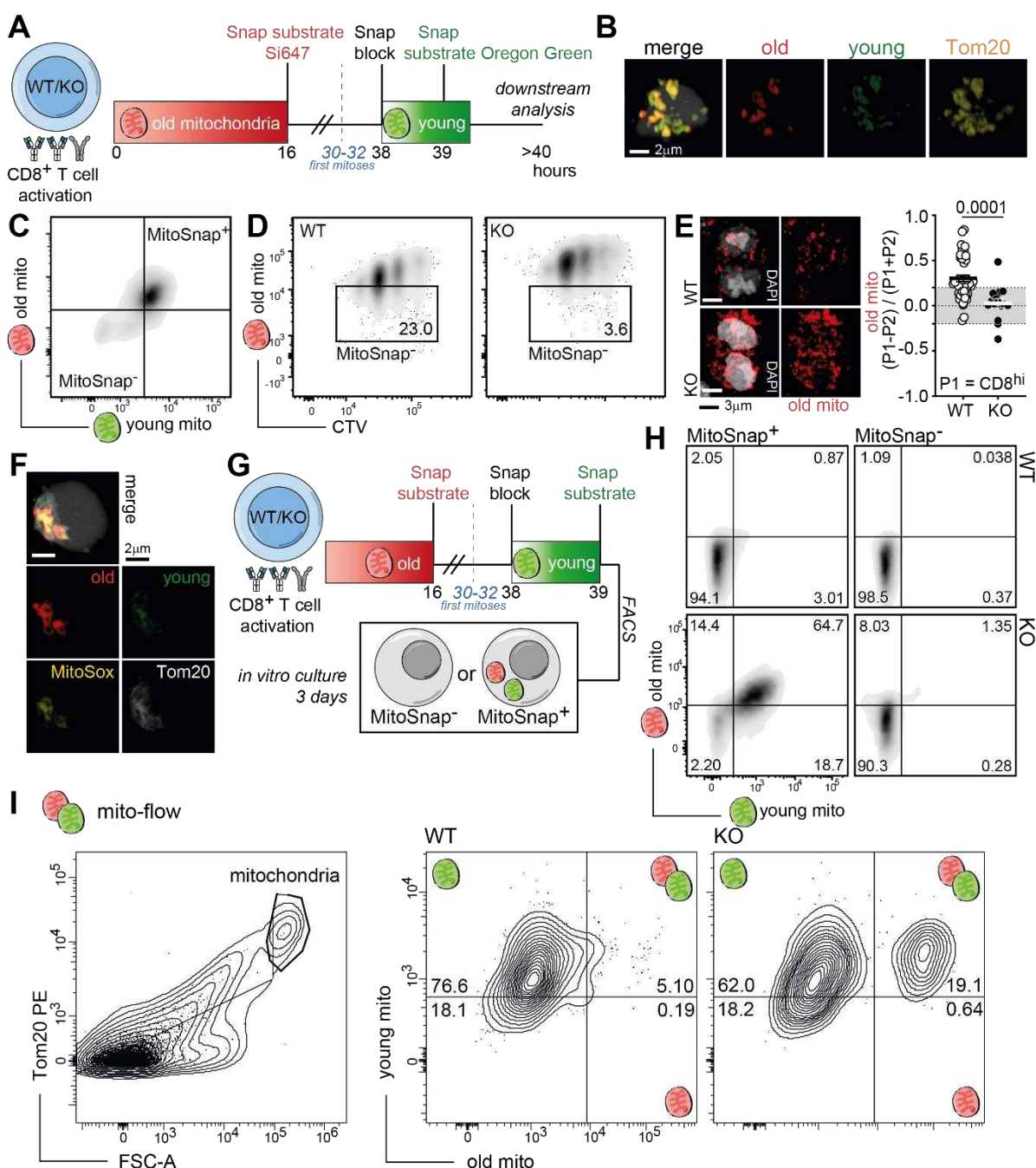
151 **Figure 1. Autophagy regulates asymmetries in CD8<sup>+</sup> T cell mitosis.** (A) Experimental layout: CTV-  
152 labelled naïve CD8<sup>+</sup> T cells were activated on anti-CD3, anti-CD28 and Fc-ICAM-1 coated plates for  
153 36-40 h. Cells were harvested and stained with anti-CD8 antibodies. First-daughter cells were identified  
154 as the first peak of CTV dilution (in reference to undivided cells). CD8<sup>hi</sup> and CD8<sup>lo</sup> cells were sorted as  
155 populations expressing 20% highest or lowest CD8, respectively, as previously described<sup>28</sup>. Cells  
156 pellets were frozen and stored until being processed for proteomics analysis. (B) Volcano plot showing  
157 differentially inherited proteins by CD8<sup>hi</sup> and CD8<sup>lo</sup> daughter-cells. Data pooled from 4 samples done in  
158 2 independent experiments. Each sample had cells originally harvested from 2-3 mice. Encoding genes  
159 for proteins amongst the top 50 differentially expressed in CD8<sup>lo</sup> and CD8<sup>hi</sup> daughter cells are  
160 highlighted in green and red, respectively. Genes in bold have their function linked to mitochondrial  
161 metabolism and function. (C) Representative transmission electron microscopy images from CD8<sup>hi</sup> and  
162 CD8<sup>lo</sup> daughter cells emerging from the first mitosis following naïve CD8<sup>+</sup> T cell activation (left). Number  
163 of mitochondria per image/slice was calculated (right). (D) Representative images of WT (*Atg16l1*<sup>fl/fl</sup>  
164 *Ert2*<sup>Cre</sup>) and autophagy KO (*Atg16l1*<sup>fl/fl</sup> *Ert2*<sup>Cre</sup>) mitotic CD8<sup>+</sup> T cells 36-40 h post-activation. Autophagy  
165 depletion was achieved by culturing cells in presence of 500 nM Z-4-Hydroxytamoxifen (4OHT). Inheritance of MitoSOX was calculated as previously described<sup>28</sup>. Any values above or below the grey  
166 area in the graph were considered asymmetric. Data are represented as mean  $\pm$  SEM. Statistical  
167

168 analysis was performed using an unpaired two-tailed Student's *t* test. Exact P values are depicted in  
169 the figure. **(E)** Representative images of mitotic CD8<sup>+</sup> T cells from young (8-16 weeks-old) and old (>100  
170 weeks-old) mice 36-40 h post-activation. Inheritance of LC3B, a marker of autophagosomes, was  
171 calculated in each group. Data are represented as mean  $\pm$  SEM. Statistical analysis was performed  
172 using an unpaired two-tailed Student's *t* test. Exact P values are depicted in the figure. **(F)** Volcano plot  
173 showing differentially inherited proteins by CD8<sup>hi</sup> and CD8<sup>lo</sup> daughter-cells from *Atg16l1<sup>fl/fl</sup> Ert2<sup>Cre</sup>* (post-  
174 tamoxifen inducible depletion of autophagy) and old (>100 weeks) mice. Data pooled from 2-4 samples.  
175 Each sample had cells originally harvested from 2-3 mice. Encoding genes for proteins amongst the  
176 top 50 differentially expressed in CD8<sup>lo</sup> and CD8<sup>hi</sup> daughter cells are highlighted in green and red,  
177 respectively, for each type of sample. Genes are ordered from top to bottom in decreasing fold-change  
178 values. Genes in bold have their function linked to mitochondrial metabolism and function. Proteomics  
179 volcano plots were done using Tableau.

180 Inheritance of old mitochondria is autophagy-dependent

181 To functionally address whether damaged organelles play a role as fate determinants during ACD *in*  
182 *vivo*, we took advantage of the MitoSnap murine model (MGI:6466976; *Omp25-SnapTag<sup>fl/fl</sup> Ert2<sup>Cre</sup>*),  
183 which allows mitochondria to be followed from the mother cell, hereafter named 'old' based on the  
184 permanent fluorescent labelling of a SnapSubstrate targeted to mitochondria via OMP25. SnapTag is  
185 a modified DNA repair enzyme that can covalently bind to different cell-permeable substrates linked to  
186 fluorophores. Sequential labelling of SnapTag expressing cells allows separation by flow cytometry of  
187 different populations based on patterns of organelle inheritance. We optimized the timelines to  
188 discriminate between older and younger organelles in CD8<sup>+</sup> T cells. Briefly, naïve CD8<sup>+</sup> T cells were  
189 isolated, activated overnight on anti-CD3, anti-CD28 and Fc-ICAM-1 coated plates in the presence of  
190 Z-4-Hydroxytamoxifen (4OHT) to induce SnapTag expression, and labelled with two different  
191 fluorescently labelled SnapSubstrates at 16 h ('old', before 1<sup>st</sup> mitosis), and 36 h ('young', post-mitotic)  
192 post-stimulation. Incubation with an unlabelled SnapSubstrate (SnapBlock) was done immediately  
193 before the second labelling, guaranteeing that young organelle structures had emerged from recent  
194 biogenesis. Downstream analysis was done 2 h post-young labelling (Fig. 2A)<sup>35,36</sup>. With the MitoSnap  
195 system we can unequivocally link the inheritance of labelled (old) mitochondria to an event of  
196 asymmetric segregation of a cell cargo that was present >24 h before cell division. Furthermore, this  
197 cargo is not affected by recent transcriptional, translational or anabolic events of biogenesis. SnapTag  
198 labelled mitochondria co-localized with Tom20+ structures by fluorescence confocal microscopy,  
199 confirming the specificity of the SnapTag chemistry (Fig. 2B). Analysis of first-daughter CD8<sup>+</sup> T cells by  
200 flow cytometry revealed the emergence of two main populations inheriting either both old and young  
201 mitochondria or exhibiting no SnapTag labelling (Fig. 2C). Importantly, SnapTag negative cells result  
202 from degradation or segregation of mitochondria, as labelling efficiency is close to 100% (Fig. S2A). To  
203 confirm whether these two populations result from segregation into the daughter cells or degradation,  
204 we generated autophagy-deficient MitoSnap mice (*Atg16l1<sup>fl/fl</sup> Omp25-SnapTag<sup>fl/fl</sup> Ert2<sup>Cre</sup>*). We labelled  
205 old SnapTag mitochondria from autophagy-sufficient and autophagy-deficient CD8<sup>+</sup> T cells and  
206 evaluated their loss over several cell divisions. Autophagy-deficient MitoSnap CD8<sup>+</sup> T cells only lost the  
207 old mitochondria in 3.6% of all dividing cells, as opposed to 23% in WT conditions (Fig. 2D). To directly  
208 observe segregation events, mitotic MitoSnap CD8<sup>+</sup> T cells were analyzed by fluorescence confocal  
209 microscopy, revealing that asymmetric segregation of old mitochondria occurs in WT but not KO cells  
210 and therefore relies on autophagy (Fig. 2E). Importantly, we confirmed that old mitochondria are  
211 MitoSOX+ (Fig. 2F). To further dissect the role of mitophagy in the generation of MitoSnap- cells, we  
212 sorted MitoSnap+ and MitoSnap- cells following first CD8<sup>+</sup> T cell division and put them back in culture  
213 without any further TCR stimulation for 3 days in T cell medium containing IL-2, IL-7 and IL-15, which  
214 are cytokines that promote survival and memory maintenance (Fig. 2G). Using MitoSnap- conditions as  
215 reference negative controls, we observed that WT cells that were originally MitoSnap+ became  
216 MitoSnap-. However, most of the MitoSnap+ autophagy-deficient CD8<sup>+</sup> T cells maintained their  
217 SnapTag labelling (Fig. 2H). Finally, aiming to comprehend the mitochondrial content of autophagy-  
218 sufficient and -deficient CD8<sup>+</sup> T cells at the organelle level, we enriched mitochondrial fractions of both  
219 types of cells at 40 h post-activation (as in Fig. 2A) and performed flow cytometry analysis. We gated  
220 on mitochondria based on their size and Tom20 expression and observed that mitochondrial units are  
221 larger in *Atg16l1*-deficient cells (Fig. 2A, Fig. S2B). Supporting the role of mitophagy in the clearance  
222 of aged mitochondria, we observed that autophagy-deficient cells had a higher proportion of

223 mitochondria preserving old organelle labelling in comparison to their WT counterparts (Fig. 2I). These  
 224 results suggest that the emergence of MitoSnap- cells relies both on segregation and degradation  
 225 events and that autophagy plays a role in both mechanisms.



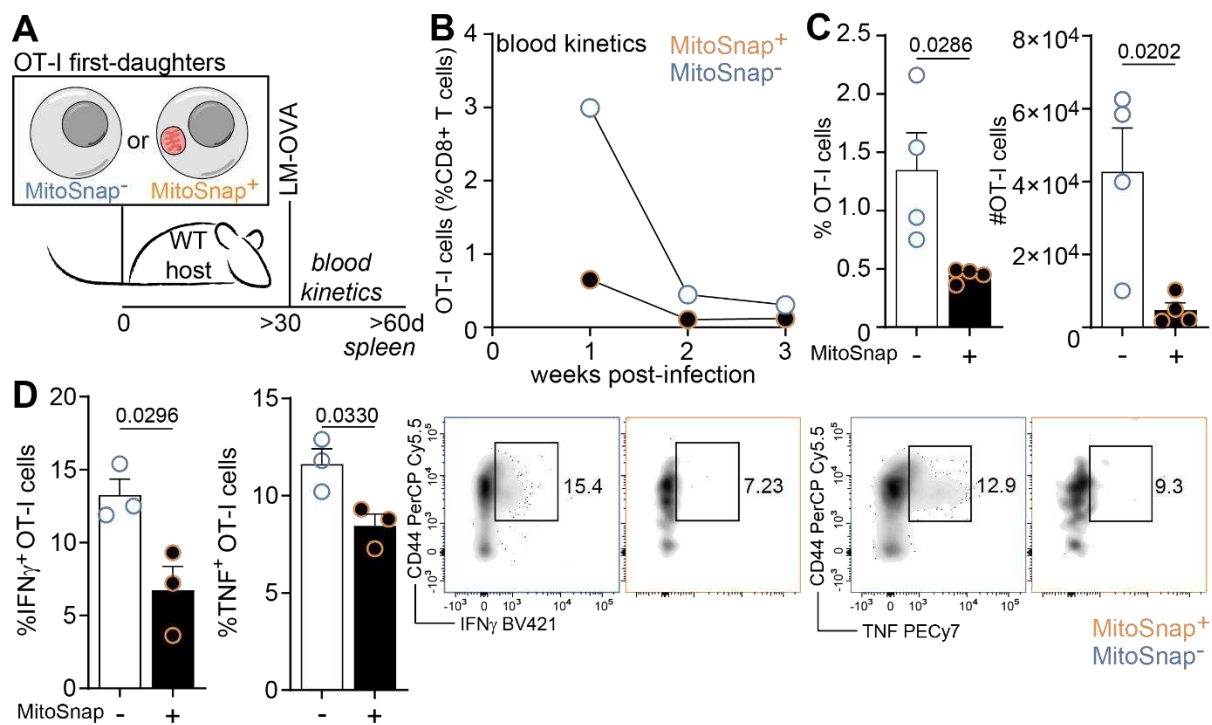
226

227 **Figure 2. Inheritance of old mitochondria is autophagy-dependent.** (A) Experimental layout: CTV  
 228 labelled naïve MitoSnap CD8<sup>+</sup> T cells (WT-*Atg16l1*<sup>fl/fl</sup> *Omp25*<sup>fl/fl</sup> *Ert2*<sup>Cre</sup> or KO-*Atg16l1*<sup>fl/fl</sup> *Omp25*<sup>fl/fl</sup> *Ert2*<sup>Cre</sup>)  
 229 were activated on anti-CD3, anti-CD28 and Fc-ICAM-1 coated plates for 36-40 h. Cells were cultured  
 230 in T cell medium containing 500 nM Z-4-Hydroxytamoxifen (4OHT). 16 h post-activation, cells were  
 231 harvested and labelled with Snap-Cell 647-SiR to tag old mitochondria and cultured for a further 24 h,  
 232 when Snap-Cell Block and Snap-Cell Oregon Green incubations allowed young organelle labelling.  
 233 Downstream analysis was done >2 h after cell resting in complete T cell medium at 37°C. (B)  
 234 Representative confocal microscopy images showing specificity of SnapTag labelling (staining overlaps  
 235 with anti-Tom20 antibody labelling) in WT MitoSnap CD8<sup>+</sup> T cells 36 h post-activation. (C)  
 236 Representative flow cytometry plot of old and young mitochondria inheritance amongst activated  
 237 MitoSnap CD8<sup>+</sup> T cells following first cell division. (D) Representative flow cytometry plots showing

238 inheritance of old mitochondria during several cell division cycles in both autophagy-sufficient (WT) and  
239 autophagy-deficient (KO) cells. **(E)** Representative confocal microscopy images of mitotic WT and KO  
240 MitoSnap CD8<sup>+</sup> T cells 36-40 h post-activation. Asymmetric inheritance of old mitochondria was  
241 calculated in each group. Data are represented as mean  $\pm$  SEM. Statistical analysis was performed  
242 using an unpaired two-tailed Student's *t* test. Exact P values are depicted in the figure. **(F)**  
243 Representative confocal microscopy images showing overlap between MitoSOX staining and old  
244 mitochondria labelling in WT MitoSnap CD8<sup>+</sup> T cells 36 h post-activation. **(G)** Experimental layout: CTV  
245 labelled MitoSnap CD8<sup>+</sup> T cells (WT-*Atg16l1*<sup>fl/fl</sup>- *Omp25*<sup>fl/fl</sup>- *Ert2*<sup>Cre</sup> or KO-*Atg16l1*<sup>fl/fl</sup> *Omp25*<sup>fl/fl</sup>- *Ert2*<sup>Cre</sup>) were  
246 activated and SnapTag labelled as in 2A. MitoSnap- cells and MitoSnap+ cells were sorted as depicted  
247 in 2C. Sorted cells were cultured for 3 days in T cell medium supplemented with IL-2, IL-7 and IL-15.  
248 **(H)** Representative plots from MitoSnap CD8<sup>+</sup> T cells 3 days post sorting. Sorted MitoSnap- cells were  
249 used to set up gating strategy. **(I)** MitoSnap CD8<sup>+</sup> T cells (WT-*Atg16l1*<sup>fl/fl</sup>- *Omp25*<sup>fl/fl</sup>- *Ert2*<sup>Cre</sup> or KO-  
250 *Atg16l1*<sup>fl/fl</sup> *Omp25*<sup>fl/fl</sup>- *Ert2*<sup>Cre</sup>) were activated and SnapTag-labelled as in 2A. Mitochondria were purified  
251 and phenotyped by flow cytometry. Mitochondrial gating was determined based on size and Tom20  
252 expression (left, also refer to Fig. S2B). SnapTag-labelling was preserved and maintenance of old and  
253 young organelle staining was evaluated in autophagy-sufficient and autophagy-deficient cells.

254 Old mitochondria are cell fate determinants that impede memory CD8<sup>+</sup> T cell differentiation

255 Next, we aimed to investigate whether the inheritance of aged mitochondria impacts the fate of CD8<sup>+</sup> T  
256 cells *in vivo*. To achieve that, we generated OT-I CD45.1 MitoSnap mice. CD8<sup>+</sup> T cells from OT-I mice  
257 express a transgenic TCR specific to OVA<sub>257-264</sub> SIINFEKL peptide<sup>37</sup>. The transgenic TCR allows robust  
258 and specific TCR-activation of these cells and CD45.1 allows tracing of these cells in a host mouse. As  
259 antigen, we chose *Listeria monocytogenes* expressing OVA (LM-OVA) as an acute infection model.  
260 OT-I MitoSnap cells were activated *in vitro* and first-daughter cells sorted into MitoSnap+ and MitoSnap-  
261 populations. These two distinct populations of OT-I T cells were transferred to WT naïve CD45.2  
262 C57BL/6 hosts and after >4 weeks host mice were infected with LM-OVA. The immune responses  
263 generated by the transferred OT-I MitoSnap cells were followed by blood kinetics and >4 weeks post-  
264 bacterial challenge (memory phase) we assessed the abundance, phenotype and function of remaining  
265 progenies (Fig. 3A). We observed that cell populations derived from originally MitoSnap- cells had  
266 superior ability to survive than those generated by from MitoSnap+ cells, as re-expansion potential upon  
267 LM-OVA infection was significantly higher in the first group (Fig. 3B). The higher frequencies of  
268 MitoSnap- progenies within the total CD8<sup>+</sup> T cell population from the host were maintained throughout  
269 the course of the immune response. When spleens were analyzed at the memory phase, we confirmed  
270 that higher frequencies were also predictive of higher OT-I cell numbers (Fig. 3C). Upon *in vitro* re-  
271 stimulation, MitoSnap- progenies also produced more than twice as much IFN $\gamma$  than their MitoSnap+  
272 counterparts (Fig. 3D). We did not observe differences in the frequencies of KLRG1<sup>+</sup>CD127<sup>+</sup> and  
273 KLRG1<sup>+</sup>CD127<sup>-</sup> between MitoSnap+ and MitoSnap- progenies (Fig. S3A). *In vitro* Tat-Cre driven  
274 recombination of *Omp25*-SnapTag<sup>fl/fl</sup>- CD8<sup>+</sup> T cells resulted in similar results, i.e. MitoSnap- cells show  
275 higher re-expansion rates upon cognate antigen re-challenge than MitoSnap+ cells (Fig. S3B).  
276 Together, the phenotype and function of MitoSnap- CD8<sup>+</sup> T cells suggest that they have better memory  
277 potential.



278

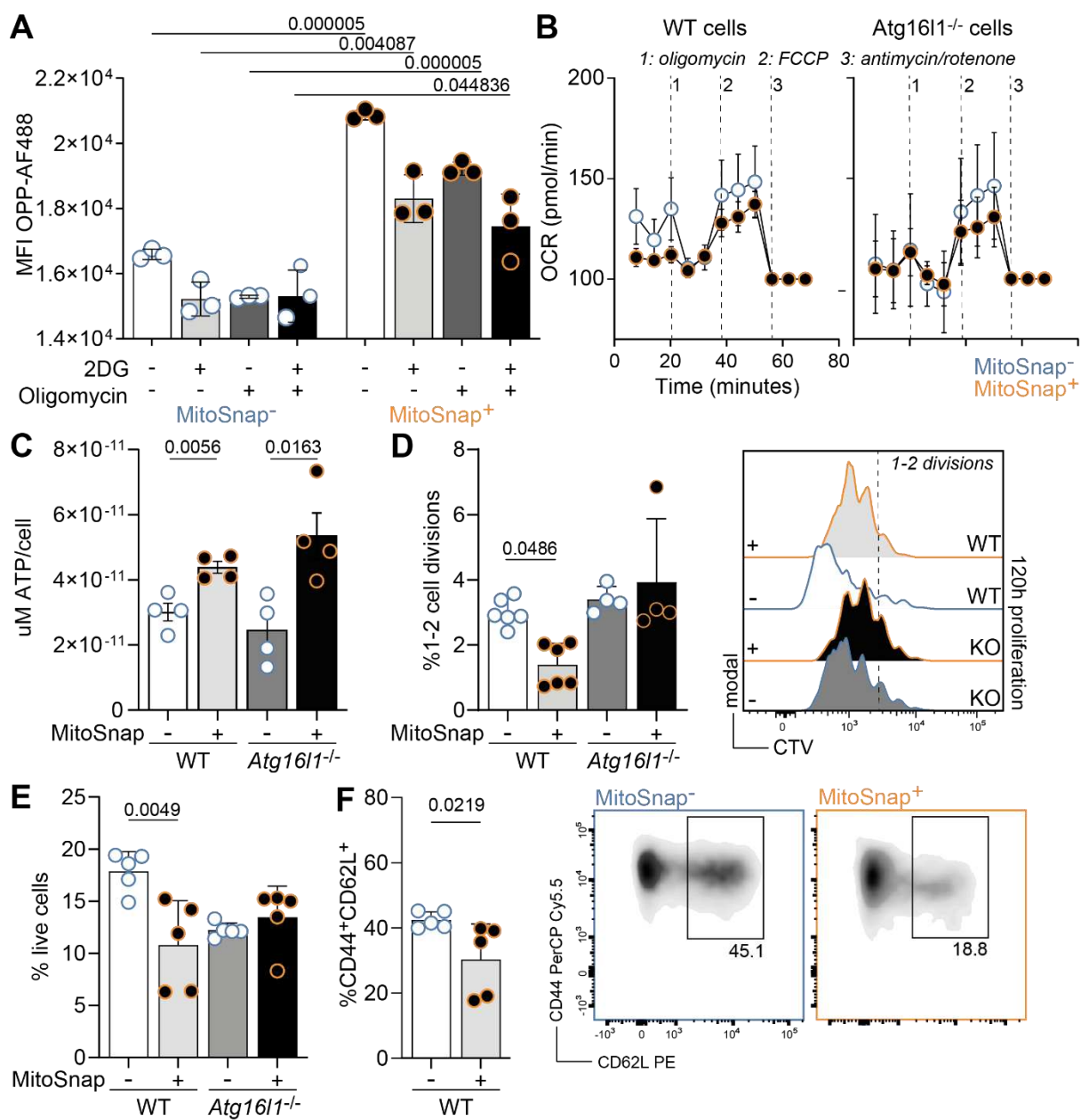
**Figure 3. Old mitochondria are cell fate determinants that impede memory CD8<sup>+</sup> T cell differentiation.** (A) Experimental layout: CTV labelled naïve OT-I MitoSnap CD8<sup>+</sup> T cells (*Atg16l1<sup>fl/fl</sup>*-*Omp25<sup>fl/fl</sup>*-*Ert2<sup>Cre</sup>*) were activated on anti-CD3, anti-CD28 and Fc-ICAM-1 coated plates for 36-40 h. Cells were cultured in T cell medium containing 500 nM Z-4-Hydroxytamoxifen (4OHT). 16 h post-activation, cells were harvested and labelled with Snap-Cell 647-SiR to tag old mitochondria and put back in culture. 24 h later cells were sorted into MitoSnap+ and MitoSnap- cells. 5x10<sup>3</sup> cells were transferred to new hosts (CD45.1 and CD45.2 congenic markers were used to trace transferred cells). >30 days following adoptive cell transfer, host mice were infected with 2000 colony forming units (CFU) of *Listeria monocytogenes* expressing ovalbumin (OVA) (LM-OVA). Immune responses were evaluated in the blood and spleen. (B) Frequencies of OT-I cells within the CD8<sup>+</sup> T-cell population in the blood. (C) Frequency and numbers of adoptively transferred OT-I cells within CD8<sup>+</sup> T cells in the spleens of recipient mice. (D) Frequency of splenic IFN $\gamma$  and TNF OT-I producing cells (left). Representative flow cytometry plots of MitoSnap+ and MitoSnap- cytokine producing cells (right). C, D: Data are represented as mean  $\pm$  SEM. Statistical analysis was performed using an unpaired two-tailed Student's *t* test. Exact P values are depicted in the figure. Representative data of 1 out of 4 experiments.

294

#### 295 Inheritance of aged mitochondria counteracts cellular quiescence

296 Effector CD8<sup>+</sup> T cells are highly proliferative, while memory CD8<sup>+</sup> T cells divide slower and are more  
 297 quiescent. This is a feature that is established early on following T cell activation, with cell cycle speed  
 298 predictive of CD8<sup>+</sup> T cell fate<sup>22,38</sup>. CD8<sup>+</sup> T cells with different clonal expansion rates have different  
 299 metabolic demands, effector cells being more reliant on glycolysis, while long-lived naïve and memory  
 300 cells mostly perform mitochondrial oxidative phosphorylation and fatty acid oxidation to produce  
 301 ATP<sup>32,33</sup>. Thus, we investigated whether the metabolism of first-daughter CD8<sup>+</sup> T cells is impacted by  
 302 the inheritance of aged mitochondria using a modified version of the Scenith assay<sup>39</sup>. This assay allows  
 303 measurement of metabolic dependencies by quantifying cellular translation rates, which highly correlate  
 304 with ATP production. Translation is measured by the incorporation of O-propargyl-puromycin (OPP, a  
 305 puromycin analogue), which can be visualized using click chemistry and flow cytometry. Metabolic  
 306 reliance is evaluated by the addition of different inhibitors targeting glycolysis or OXPHOS. MitoSnap+  
 307 CD8<sup>+</sup> T cells inheriting old mitochondria exhibited higher global translation rates and reliance on  
 308 glycolysis than MitoSnap- cells, which were more metabolically quiescent (Fig. 4A). Because the  
 309 resolution of this assay did not allow us to quantify mitochondrial function in MitoSnap- cells, we also

310 directly measured oxygen consumption rates (OCR, Fig. 4B) and ATP synthesis (Fig. 4C) in both  
311 purified populations. Besides a trend of higher basal respiration in MitoSnap- cells, we did not observe  
312 significant differences between the two populations (Fig. S4A). We speculate that differences in  
313 mitochondrial respiration were not seen because defects in mitochondrial function might take longer  
314 than a timeline of 24 h, the time between old-organelle labelling and the experimental assay. We did  
315 the same metabolic measurements in autophagy-deficient MitoSnap+ and MitoSnap- cells, and  
316 obtained similar results (Fig 4B-C, S4A). To assess whether inheritance of distinct mitochondrial pools  
317 and differences in metabolic reliance cause differences in proliferation rates and survival, sorted  
318 MitoSnap+ and MitoSnap- cells were cultured in T cell medium containing IL-2, IL-7 and IL-15 in  
319 absence of T cell activation for further 3 or 7 days, respectively. CD8+ T cells inheriting aged  
320 mitochondria exhibited lower frequencies of slow-dividing cells, and more homogeneous proliferation  
321 profile in comparison to MitoSnap- cells, corroborating their less quiescent status that might contribute  
322 to precocious cell death (Fig. 4E). Autophagy-deficient cells showed slower proliferation rates  
323 independent of their mitochondrial inheritance profile, suggesting that autophagy loss might play a role  
324 in cell cycle arrest, which corroborates previous reports about the role of autophagy in degrading cyclin-  
325 dependent kinase inhibitor 1B (CDKN1B) in T cells<sup>40</sup>. Concerning survival in cytokine-limiting  
326 conditions, as expected for the effector population, MitoSnap+ cells showed lower viability than  
327 MitoSnap- cells after 7 days in culture (Fig. 4F). Interestingly, autophagy-sufficient remaining surviving  
328 cells exhibited distinct phenotypes, being CD44+CD62L+ cells, an expression pattern seen quiescent  
329 memory cells<sup>22,38</sup>, more abundant amongst MitoSnap- progenies (Fig. 4G). Autophagy-deficient cells  
330 did not exhibit differences in phenotype linked to early mitochondrial inheritance (Fig. S4B). Because in  
331 WT cells aged mitochondria are cleared after 3 days even in MitoSnap+ cells that inherited their  
332 mitochondria from the mother cell, our results suggest that old organelles inherited at first division  
333 counteract cellular quiescence at early stages post-T cell stimulation. In turn this promotes the  
334 emergence of a cell population that resembles short-lived effector CD8+ T cells. Our results provide the  
335 first unequivocal data linking organelle inheritance in mammals - here mitochondria - to changes in cell  
336 function that culminate in fate commitment of cells *in vivo*.



337

338 **Figure 4. Inheritance of aged mitochondria counteracts cellular quiescence.** (A) CTV labelled  
339 naïve MitoSnap CD8+ T cells (*Atg16l1<sup>fl/fl</sup> Omp25<sup>fl/fl</sup> Ert2<sup>Cre</sup>*) were activated on anti-CD3, anti-CD28 and  
340 Fc-ICAM-1 coated plates for 36-40 h. Cells were cultured in T cell medium containing 500 nM Z-4-  
341 Hydroxytamoxifen (4OHT). 16 h post-activation, cells were harvested and labelled with Snap-Cell 647-  
342 SiR (old mitochondria) and cultured for further 24 h, when cells were harvested and prepared for the  
343 Scenith assay to evaluate their metabolic reliance. OPP incorporation was used as a readout of  
344 translation. 2-Deoxy-D-glucose was used to inhibit glycolysis and oligomycin was used to inhibit  
345 mitochondrial respiration. A combination of both inhibitors was used to suppress both metabolic  
346 pathways and obtain an OPP baseline. Analysis was done by flow cytometry, which allowed the  
347 discrimination of MitoSnap+ and MitoSnap- cells. Data are represented as mean ± SEM. Statistical  
348 analysis was performed using Two-Way ANOVA with Tukey's post-hoc test. Exact P values are  
349 depicted in the figure. Representative data of 1 out of 3 experiments. (B) Oxygen consumption rate  
350 (OCR) of sorted MitoSnap+ and MitoSnap- first-daughter CD8+ T cells was measured under basal  
351 conditions and in response to indicated drugs. Data are represented as mean ± SEM. Datapoints  
352 represent 4 technical replicates from 2 biological samples. (C) ATP production by sorted MitoSnap+  
353 and MitoSnap- first-daughter CD8+ T cells originally isolated from WT (*Atg16l1<sup>fl/fl</sup> Omp25<sup>fl/fl</sup> Ert2<sup>Cre</sup>*) or  
354 KO (*Atg16l1<sup>fl/fl</sup> Omp25<sup>fl/fl</sup> Ert2<sup>Cre</sup>*) mice. Data are represented as mean ± SEM. Statistical analysis was

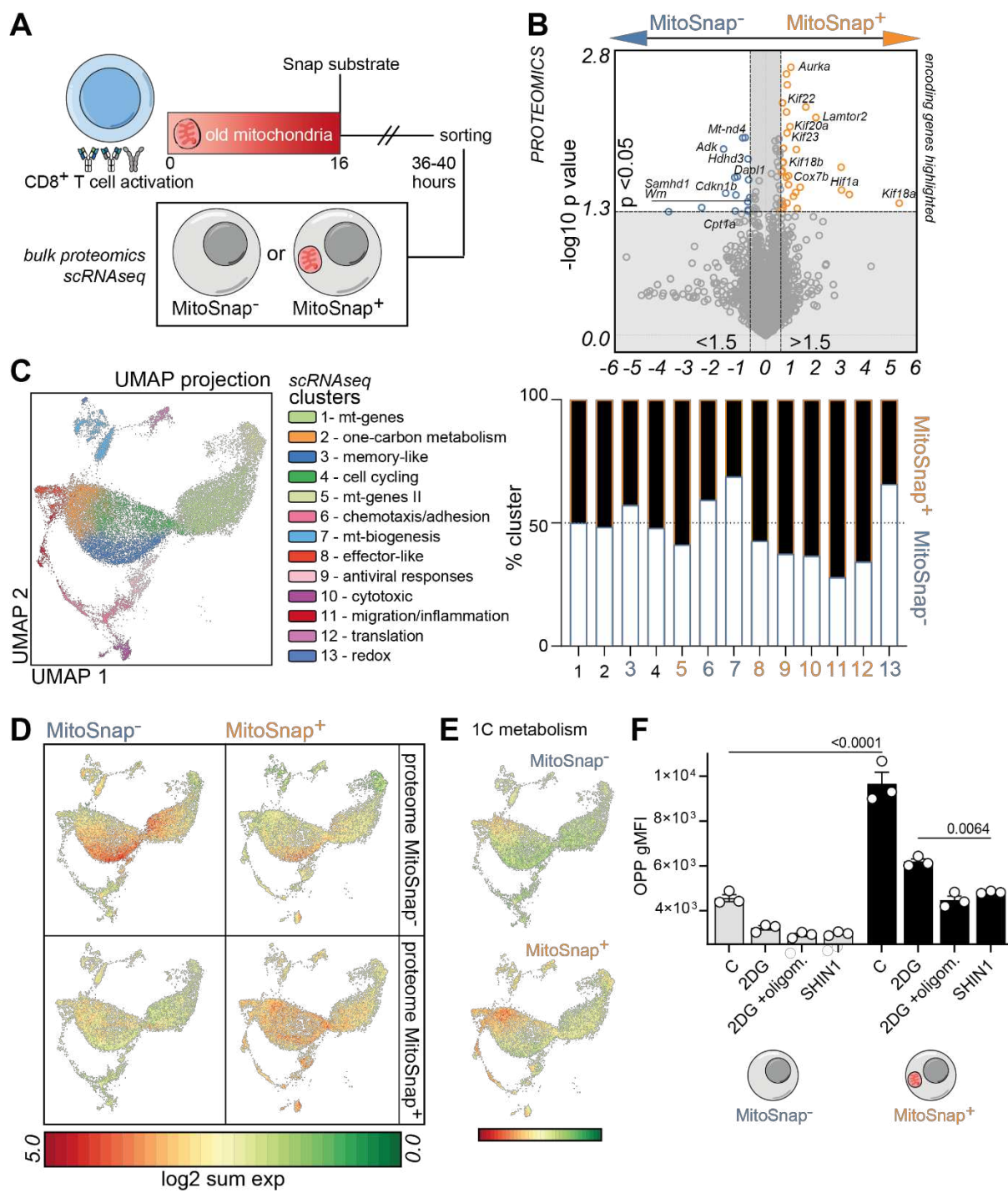
355 performed using an unpaired two-tailed Student's *t* test. Exact P values are depicted in the figure.  
356 Datapoints represent 4 technical replicates from 1 biological sample per group. Representative data  
357 from 1 out of 2 experiments. **(D)** WT and KO MitoSnap+ and MitoSnap- cells were sorted as  
358 represented in figure 2G and cultured for 3 days in T cell medium supplemented with IL-2, IL-7 and IL-  
359 15. Frequency of slow-dividing cells (1 or 2 divisions) was calculated. Data are represented as  
360 mean  $\pm$  SEM. Statistical analysis was performed using One-Way ANOVA. Exact P values are depicted  
361 in the figure. Datapoints represent 1-3 technical replicates from 2 biological samples per group.  
362 Representative data from 1 out of 2 experiments. **(E)** WT and KO MitoSnap+ and MitoSnap- cells were  
363 sorted as represented in figure 2G and cultured for 7 days in T cell medium supplemented with IL-2, IL-  
364 7 and IL-15. Frequency of viable cells was calculated. Data are represented as mean  $\pm$  SEM. Statistical  
365 analysis was performed using One-Way ANOVA. Exact P values are depicted in the figure. Datapoints  
366 represent 5 technical replicates from 1 biological sample per group. Representative data from 1 out of  
367 2 experiments. **(F)** Frequency of CD44+ CD62L+ cells within surviving cells from E was calculated.  
368 Gating strategy is depicted (right panel). Data are represented as mean  $\pm$  SEM. Statistical analysis was  
369 performed using an unpaired two-tailed Student's *t* test. Exact P values are depicted in the figure.  
370 Datapoints represent 5 technical replicates from 1 biological sample per group. Representative data  
371 from 1 out of 2 experiments.

372

373 Unequal inheritance of mitochondrial populations drives changes in the transcriptome and proteome of  
374 CD8+ T cells

375 Aiming to further identify the fate-divergency drivers found in cells and the metabolism of daughter cells  
376 inheriting distinct mitochondrial pools, we labelled old mitochondria in activated CD8+ T cells, sorted  
377 MitoSnap+ and MitoSnap- first-daughter cells and performed single-cell transcriptomics (scRNAseq)  
378 and bulk proteomics analysis of these two populations (Fig. 5A). Proteomics analysis of combined 4  
379 experiments (6 samples per group) allowed us to identify a small list of differentially inherited proteins  
380 in these two populations. MitoSnap- cells expressed higher levels of Werner protein (WRN), an enzyme  
381 important for genome stability<sup>41</sup>, and NADH dehydrogenase 4 (mt-ND4), a protein involved in  
382 mitochondrial biogenesis as part of the mitochondrial respiratory chain complex I (gene ID: 4538,  
383 HGNC). MitoSnap+ cells were enriched in Hypoxia Inducible Factor 1 Subunit Alpha (HIF1a) and late  
384 endosomal/lysosomal adaptor 2 (LAMTOR2), proteins involved in mammalian target of rapamycin  
385 (mTOR) metabolism, which has been reported to boost effector CD8+ T cell differentiation<sup>42,43</sup> (Fig. 5B).  
386 In other studies, including our own, transcriptional profiling of CD8+ T cell populations following one  
387 cycle of cell division was performed using bulk and single cell strategies<sup>27-30,44</sup>. However, these reports  
388 either relied on the expression of surface markers and reporter genes with the caveat of their dynamic  
389 expression to identify effector-like and memory-like cell daughters. They could not directly link the  
390 transcriptional divergences to asymmetric inheritance of cell fate determinants during mitosis, as cells  
391 were generated *in vivo* and could have emerged from both symmetric and asymmetric cell divisions.  
392 Unbiased clustering of single cell transcriptomes and visualization with uniform manifold approximation  
393 and projection (UMAP) plots, allowed us to define 15 clusters (Fig. 5C). Both types of cells were present  
394 in all clusters, but some were enriched in MitoSnap+ or MitoSnap- daughter-cells. By evaluating the  
395 expression of the genes encoding for proteomics enriched targets in our scRNAseq UMAP, we  
396 confirmed that there was a positive correlation between gene and protein expression. Furthermore, the  
397 MitoSnap+ proteome cluster was enriched in clusters 1 (lower-half), 2, 4 and 8-12, while the MitoSnap-  
398 proteome cluster was enriched in clusters 1 (upper-half), 3, 7 and 13 (Fig. 5D). Interestingly, these  
399 cluster regions matched MitoSnap+ and MitoSnap- enriched clusters concerning cell numbers (Fig. 5C).  
400 Based on the genes mostly expressed in each cluster, we could assign functional signatures to each of  
401 them. Clusters 1 and 5 exhibited very high expression of mitochondrial encoded genes. Clusters  
402 dominated by MitoSnap- cells showed a memory-related signature (Cluster 3), high expression of genes  
403 linked to mitochondrial function and biogenesis (Cluster 7) and redox balance (Cluster 13) or a  
404 transcriptional signature marked by genes involved in chemotaxis and adhesion (Cluster 6). Most of the  
405 other clusters had a majority of MitoSnap+ cells and exhibited transcriptional profiles that could be  
406 linked to effector functions (Clusters 8-12). These gene signatures are aligned with the functional  
407 readouts previously obtained, as MitoSnap- cells are the ones with higher mitochondrial turnover rates  
408 and memory potential, while MitoSnap+ cells are more proliferative and show lower survival rates in

409 absence of TCR-stimulation, a feature of effector-like cells. We also selected genes extensively  
410 reported to promote effector or memory differentiation in CD8<sup>+</sup> T cells and found that they were enriched  
411 in MitoSnap+ and MitoSnap- abundant clusters, respectively (Fig. S5A-C). Interestingly, we also found  
412 a cluster enriched in genes that are linked to one-carbon (1C) metabolism (e.g. *Mthfd2*, *Phgdh* and  
413 *Shmt2*, Cluster 2, Fig. S5D). This cluster is formed by a small majority of MitoSnap+ cells, but the 1C  
414 metabolism signature is stronger in this population in comparison to MitoSnap- cells (Fig. 5E). In CD4<sup>+</sup>  
415 T cells 1C metabolism is essential for proliferation and effector function as an inducer of mTOR  
416 activity<sup>45</sup>. Thus, aiming to functionally validate this finding, we again measured metabolic reliance  
417 through Scenith using SHIN, an inhibitor of serine hydroxymethyltransferase (SHMT1/2) activity, a  
418 mitochondrial enzyme responsible for the catabolism of serine to glycine, key to one-carbon  
419 metabolism. Our results suggest that in MitoSnap+ cells SHIN1 treatment indeed suppresses their  
420 translation rates, a phenotype that was not shared by MitoSnap- cells (Fig. 5F). Taken together, these  
421 results further support that inheritance of mitochondrial pools of different ages determines T cell fate  
422 divergence and this is caused by distinct strategies to fulfil metabolic demands: MitoSnap- cells are  
423 more quiescent and quickly turn over mitochondria, which includes mitochondrial biogenesis, while  
424 MitoSnap+ cells keep old/damaged mitochondria, are more glycolytic and turn to one-carbon  
425 metabolism, one of the first consequences after a mitochondrial insult.



426

427 **Figure 5. Unequal inheritance of mitochondrial populations drives changes in the transcriptome**  
428 **and proteome of CD8<sup>+</sup> T cells.** (A) Experimental layout: CTV labelled naïve MitoSnap CD8<sup>+</sup> T cells  
429 (*Atg16l1*<sup>fl/fl</sup> *Omp25*<sup>fl/fl</sup> *Ert2*<sup>Cre</sup>) were activated on anti-CD3, anti-CD28 and Fc-ICAM-1 coated plates for  
430 36-40 h. Cells were cultured in T cell medium containing 500 nM Z-4-Hydroxytamoxifen (4OHT). 16 h  
431 post-activation, cells were harvested and labelled with Snap-Cell 647-SiR (old mitochondria) and  
432 cultured for further 24 h. Cells were harvested and sorted into MitoSnap+ and MitoSnap- populations  
433 and their proteome and transcriptome were analyzed. (B) Volcano plot showing differentially inherited  
434 proteins by MitoSnap+ and MitoSnap- cells. Data pooled from 6 samples done in 4 independent  
435 experiments. MitoSnap+ and MitoSnap- enriched proteins (represented by their encoding genes) are  
436 highlighted in orange and blue, respectively. Proteomics volcano plot was done using Tableau. (C)  
437 UMAP and clustering of integrated MitoSnap+ and MitoSnap- cells obtained from 5 mice per group  
438 (left). Frequency of MitoSnap+ and MitoSnap- cells per cluster (right). (D) Genes encoding for proteins

439 enriched in MitoSnap+ or MitoSnap- were projected onto UMAP clusters from 5C. **(E)** Genes involved  
440 in one-carbon (1C) metabolism were projected onto UMAP clusters. **(F)** CTV labelled naïve MitoSnap  
441 CD8+ T cells (*Atg16l1<sup>fl/fl</sup>*; *Omp25<sup>fl/fl</sup>*; *Ert2<sup>Cre</sup>*) were activated on anti-CD3, anti-CD28 and Fc-ICAM-1 coated  
442 plates for 36-40 h. Cells were cultured in T cell medium containing 500 nM Z-4-Hydroxytamoxifen  
443 (4OHT). 16 h post-activation, cells were harvested and labelled with Snap-Cell 647-SiR (old  
444 mitochondria) and cultured for further 24 h, when cells were harvested and prepared for the Scenith  
445 assay, aiming to evaluate their metabolic reliance. OPP incorporation was used as a readout of  
446 translation. 2-Deoxy-D-glucose was used to inhibit glycolysis and oligomycin was used to inhibit  
447 mitochondrial respiration. A combination of both inhibitors was used to suppress both metabolic  
448 pathways and obtain an OPP baseline. SHIN1 was used to inhibit enzymes SHMT1/2. Analysis was  
449 done by flow cytometry, which allowed the discrimination of MitoSnap+ and MitoSnap- cells. Data are  
450 represented as mean  $\pm$  SEM. Statistical analysis was performed using Two-Way ANOVA with Tukey's  
451 post-hoc test. Exact P values are depicted in the figure. Representative data of 1 out of 2 experiments.

## 452 Discussion

453 Most of the previous functional readouts evaluating the role of ACD in early fate decisions have relied  
454 on sorting daughter cells based on the expression of the surface marker CD8 or the transcription factor  
455 c-Myc, with CD8<sup>hi</sup>/c-Myc<sup>hi</sup> cells being effector-like and CD8<sup>lo</sup>/c-Myc<sup>lo</sup> cells being memory-like  
456 progenies<sup>21,23,26</sup>. However, the expression of these molecules is highly dynamic and does not  
457 necessarily result from asymmetric segregation events. A recent pioneering study used genetic  
458 barcoding to evaluate the transcriptome of genuine sister cells and demonstrated that early-fate  
459 trajectories can be established since first CD8+ T cell division<sup>27</sup>. However, overall there is no currently  
460 existing evidence to directly link this divergence to the inheritance of a fate determinant. Here we are  
461 first to show that asymmetric inheritance of pre-mitotic cell cargo causes divergent T cell fate  
462 commitment. This was possible because the MitoSnap system allows discrimination between events of  
463 inheritance and recent biogenesis. Tagging mitochondria before mitosis can be exclusively allocated to  
464 the pre-mitotic mother cell, thus guaranteeing that post-mitotic changes in cell phenotype do not  
465 interfere with its inheritance pattern, something which was not achieved in previous reports using  
466 expression of surface markers or reporter genes.

467 Mitochondria are organelles required to meet the cell's energetic demands. They are the site of  
468 oxidative phosphorylation (OXPHOS), tricarboxylic acid (TCA) cycle and fatty acid oxidation (FAO),  
469 pathways involved in the generation of adenosine triphosphate (ATP). They are also involved in  
470 maintaining the redox balance of the cell, as they can produce reactive oxygen species (ROS), are  
471 involved in calcium signalling, can drive apoptotic cell death and, by being core metabolic modulators,  
472 also contribute to epigenetic regulation of cell function<sup>5,46</sup>. The results from several studies provide  
473 evidence that T cell fate is influenced by mitochondrial homeostasis, architecture and function: effector  
474 cells are highly glycolytic and memory cells rely on FAO<sup>32,33,47,48</sup>. Accordingly, mitochondrial quality  
475 control plays an important role in T cell fate decisions with mitophagy being a crucial regulator of cell  
476 survival<sup>17,49,50</sup>. Thus, mitochondria constitute a suitable cell cargo to be linked to differentiation  
477 trajectories, which was corroborated by our initial proteomics screening identifying mitochondrial-related  
478 proteins being differentially enriched in memory-like and effector-like CD8+ T cell daughters.

479 The emergence of cells that maintain or lose their MitoSnap labelling during CD8+ T cell proliferation  
480 could result from different cell biological processes and we dissected the mechanisms underlying the  
481 inheritance of mitochondria from the mother cell. Firstly, we identified that asymmetric cell division  
482 contributes to the polarized inheritance of old mitochondria. However, we observed that progenies able  
483 to clear old mitochondria also rapidly lost their labelling for young mitochondria, suggesting that  
484 MitoSnap- cells emerge from both segregation and degradation events, mitophagy levels being higher  
485 in this population. Autophagy and mitophagy support memory CD8+ T cell responses, but it remained  
486 unclear when these mechanisms are required to contribute to the formation of memory-precursors or  
487 the maintenance of long-lived cells<sup>15-17</sup>. To address whether autophagy plays a role in unequal  
488 mitochondrial inheritance, we used autophagy-deficient cells and found that asymmetric inheritance of  
489 old mitochondria was impaired and, as opposed to autophagy-competent cells, old mitochondria were  
490 kept for several days. These results and the symmetric proteome of CD8<sup>hi</sup> and CD8<sup>lo</sup> progenies from  
491 autophagy-deficient or old CD8+ T cells, corroborate our initial hypothesis and place ACD and

492 autophagy/mitophagy as mechanisms that work synergistically to promote early asymmetric inheritance  
493 of cell fate determinants.

494 By following the frequencies of cells inheriting or not old mitochondria (MitoSnap+/-) over the course of  
495 the immune responses it became clear that MitoSnap- cells were more functional memory cells, as they  
496 showed better maintenance, re-expansion potential and ability to produce effector-cytokines upon re-  
497 stimulation. This resembles results obtained for CD8<sup>hi</sup>/c-Myc<sup>hi</sup> and CD8<sup>lo</sup>/c-Myc<sup>lo</sup> cells<sup>21,26</sup>, with the  
498 advantage that we can finally draw a definitive link between the inheritance of a cell cargo that already  
499 existed in the mother cell to the biased fate of its progenies. We then directed our attention to determine  
500 what drives the different fates of MitoSnap+ and MitoSnap- cells. By using sorted populations or  
501 approaches that provide single-cell resolution, we determined that the metabolism, survival and  
502 proliferative capacity of these progenies is different. Exhibiting lower translation rates, higher  
503 frequencies of slow-dividing cells and CD62L expression and better survival capacity in absence of  
504 antigen, MitoSnap- cells clearly showed a stronger memory phenotype than MitoSnap+ cells<sup>22,38</sup>.  
505 Although, surprisingly, we could not observe significant differences in mitochondrial respiration rates,  
506 MitoSnap+ cells relied more on glycolysis, a feature seen in effector CD8<sup>+</sup> T cells. As old organelles  
507 also produced mitochondrial ROS as measured by MitoSOX, it is reasonable to assume that they have  
508 deteriorated mitochondrial fitness and that this might promote their early shift towards glycolysis<sup>32</sup>.  
509 Mitophagy has recently been reported to contribute to memory CD8<sup>+</sup> T cell formation<sup>17</sup>. Our results add  
510 to this, showing that mitophagy contributes to the decision for memory CD8<sup>+</sup> T cell fate commitment as  
511 early as the first mitosis following CD8<sup>+</sup> T cell stimulation, as directly measured by the loss of young  
512 mitochondria generated after the first mitosis in MitoSnap- cells.

513 Finally, to obtain an unbiased overview of the differences between MitoSnap- and MitoSnap+ cells  
514 following the first mitosis post naïve CD8<sup>+</sup> T cell activation, we performed both bulk proteomics and  
515 single cell transcriptomics of these two populations. In line with our expectations, we observed proteins  
516 linked to effector cell fate decision in MitoSnap+ cells and proteins linked to DNA health and  
517 mitochondrial biogenesis in MitoSnap- cells. It also came to our attention that a long list of kinesins (Kif  
518 genes) was enriched in effector-like MitoSnap+ daughters. Kinesins are motor proteins directly involved  
519 in intracellular trafficking of cell components along microtubules, which is important for organelle  
520 movement and for cell division events<sup>51</sup>, which fits with their less quiescent status and with the  
521 polarization of autophagosomes and mitochondria towards MitoSnap+ cells. Single cell transcriptomics  
522 allowed us to identify clusters that were enriched in MitoSnap+ and MitoSnap- cells. The presence of a  
523 memory-like cluster enriched in MitoSnap- cells, where this signature was stronger than in MitoSnap+  
524 cells, further cements this cell type as the one inheriting the memory potential.

525 We became particularly interested in a cluster with a signature enriched in MitoSnap+ cells with higher  
526 expression of genes involved in 1C metabolism. 1C metabolism comprises methionine and folate cycles  
527 that provide 1C units to boost *de novo* synthesis of nucleotides and promote amino acid homeostasis  
528 and redox defence, particularly important in dividing cells such as cancer cells<sup>52</sup>. Enzymes involved in  
529 1C metabolism can be found in the cytoplasm and the mitochondria, and both sets were upregulated in  
530 MitoSnap+ cells. Serine is an important donor of the 1C units when it is converted to glycine and in  
531 CD8<sup>+</sup> T cells this amino acid has been shown to be important for clonal expansion of effector cells<sup>53</sup>.  
532 1C metabolism has also been directly investigated in different CD4<sup>+</sup> T cell subsets and results support  
533 its role in mTOR activation and the establishment of pro-inflammatory and highly proliferative  
534 populations<sup>45</sup>. Because expression of several amino acid transporters, including serine transporters, is  
535 upregulated in MitoSnap+ cells, which also exhibit defective translation upon C1 metabolism inhibition,  
536 our results provide further evidence of the role of this pathway as a regulator of cell fate decision.

537 Collectively, our results support the notion that organelle inheritance plays an important role in CD8<sup>+</sup> T  
538 cell fate decision and contributes to the metabolic status of cell progenies. In cells from the  
539 haematopoietic lineage, the polarized presence of organelles during mitosis followed by long-term  
540 quantitative single-cell imaging has been reported, with the caveat that they were identified by dyes or  
541 probes that limit interpretation about their inheritance<sup>54</sup>. In CD8<sup>+</sup> T cells, asymmetric mTOR activity in  
542 effector-like daughter cells has been linked to its translocation to lysosomes and amino acid sensing,  
543 but *in vivo* function readouts relied on correlative CD8 expression<sup>43</sup>. Concerning the asymmetric  
544 partitioning of degradation pathways, proteasome activity has been shown to contribute to distinct T-

545 bet distribution between daughter cells, but results were not directly linked to *in vivo* T cell fates<sup>24</sup>. Here  
546 we show that organelle inheritance results from both degradation and segregation and that mitophagy  
547 and ACD work synergistically to form early memory-like cells and effector-like cells. As cells inheriting  
548 (or not) aged organelles are endowed with distinct metabolic signatures, our results suggest that  
549 therapeutic modulation of T cells can have different outcomes depending on when it is performed. Pre-  
550 mitotic modulation will globally impact on T cell differentiation, and post-mitotic approaches can  
551 selectively target a certain cell type, memory or effector, by inhibiting or improving its function. We  
552 anticipate that these findings will be relevant to a better understanding of how T cell diversity is early-  
553 imprinted and to foster the development of more efficient therapeutic strategies in the context of  
554 regenerative medicine and vaccination, which are particularly important in the context of ageing.

555 **Methods**

556 Study design

557 This study aimed to evaluate whether organelle inheritance controls CD8<sup>+</sup> T cell differentiation. To  
558 achieve that, we investigated the role of asymmetric cell division and autophagy in patterns of  
559 mitochondria inheritance. The novel MitoSnap model was used to allow specific tracking of old vs.  
560 young organelles. We used imaging analysis of mitotic CD8<sup>+</sup> T cells, flow cytometry readouts that allow  
561 single cell resolution, metabolic analysis and unbiased OMICS approaches to measure differences in  
562 phenotype and function between MitoSnap- and MitoSnap+ progenies. We used adoptive cell transfers  
563 of TCR-transgenic OT-I MitoSnap cells coupled to *Listeria monocytogenes*-OVA infections as a tool to  
564 assess immune responses and the impact of old organelle inheritance *in vivo*. All conclusions rely on  
565 at least two experiments. Every group consisted of at least two mice. No randomization or blinding was  
566 used.

567 Animal models

568 All animal work was reviewed and approved by Oxford Ethical committee and the UK Home office under  
569 the project licenses PPL30/3388 and P01275425. Mice were bred under specific pathogen-free (SPF)  
570 conditions in-house, housed on a 12 h dark:light cycle, with a 30 min period of dawn and dusk and fed  
571 ad libitum. The temperature was kept between 20 and 24 °C, with a humidity level of 45–65%. Housing  
572 cages were individually ventilated and provided an enriched environment for the animals. MitoSnap  
573 mice (MGI:6466976; *Omp25-SnapTag*<sup>f/f</sup>) were kindly provided by the lab of Prof. Pekka Katajisto. This  
574 strain was then bred with CD45.1 *Atg16l1*<sup>f/f</sup> *Ert2*<sup>Cre</sup> OT-I mice expressing a TCR specific for OVA<sub>257–264</sub>  
575 SIINFEKL peptide<sup>37</sup>, and maintained as CD45.1 or CD45.1/2 mice. Host mice in adoptive transfer  
576 experiments were either B6.SJL.CD45.1 or C57BL/6 naïve mice. Six-to-sixteen-week-old mice were  
577 considered young and > 100 week-old mice were considered aged.

578 CD8<sup>+</sup> T cell isolation and activation

579 Spleen and inguinal lymph nodes were harvested. Single-cell suspensions were used for naïve CD8<sup>+</sup>  
580 T cell isolation using EasySep™ Mouse Naïve CD8<sup>+</sup> T Cell Isolation Kit (Stemcell™ Technologies)  
581 following manufacturer's instructions. Purified populations were cultured (at 37°C, 5% CO<sub>2</sub>) in T cell  
582 medium: RPMI-1640 containing HEPES and l-glutamine (R5158, Sigma-Aldrich) supplemented with  
583 10% filtered fetal bovine serum (Sigma-Aldrich), 1× Penicillin-Streptomycin (Sigma-Aldrich), 1× non-  
584 essential amino acids (Gibco), 50 µM β-mercaptoethanol (Gibco), and 1 mM sodium pyruvate (Gibco).  
585 T cell activation was done on anti-CD3 (5 µg/ml) (145-2C11, BioLegend), anti-CD28 (5 µg/ml) (37.51,  
586 BioLegend) and recombinant human or murine Fc-ICAM-1 (10 µg/ml) (R&D Systems) coated plates.  
587 36–40h post activation cells were used in downstream assays. Autophagy deletion and/or SnapTag  
588 expression were induced by culturing cells in presence of 500 nM (Z)-4-hydroxytamoxifen (Sigma-  
589 Aldrich, H7904-5MG). To determine cell division events, cells were stained with CellTrace Violet™ (Life  
590 Technologies) following manufacturer's guidelines.

591 SnapTag labelling protocol

592 MitoSnap CD8<sup>+</sup> T cells were labelled in 1 or 3 steps. Labelling of old organelles was done by harvesting  
593 CD8<sup>+</sup> T cells 12–16 h post-activation and washing them in PBS (500 xg). Cells were incubated in T cell  
594 medium containing the first SnapSubstrate for 30 min at 37°C, washed in PBS and put back in culture

595 in their original wells for further 20-24 h. When young organelle labelling was also performed, cells were  
596 harvested, washed and incubated with T cell medium containing 5  $\mu$ M (Snap-Cell Block S9106S, New  
597 England Biolabs, NEB) for 30 min at 37°C. After washing, cells rested for 30-60 min in T cell medium  
598 and then incubated with the second SnapSubstrate for 30 min at 37°C. Fluorescent cell permeable  
599 Snap-Cell substrates (NEB) were used in the following concentrations: 3  $\mu$ M (Snap-Cell 647-SiR  
600 S9102S), 3  $\mu$ M (Snap-Cell TMR-Star S9105S), 5  $\mu$ M (Snap-Cell Oregon Green S9104S).

601 Cell survival and proliferation assays

602 Following activation, isolated MitoSnap CD8<sup>+</sup> T cells (wild type vs. ATG16L1-deficient or MitoSnap+ vs.  
603 Mito Snap- first-daughter cells) were cultured in T cell medium supplemented with murine IL-2, IL-7 and  
604 IL-15 (5 ng/ml). Cell proliferation was evaluated 3 days later and cell survival was assessed 7 days  
605 later.

606 Adoptive transfer and immunization

607 5-50 $\times$ 10<sup>3</sup> FACS-purified MitoSnap+ or MitoSnap- cells (equal numbers in the same experiment to allow  
608 comparison between the two groups) were intravenously injected into naïve recipients. In the following  
609 day, mice were infected with 2 $\times$ 10<sup>3</sup> colony-forming units (cfu) of *Listeria monocytogenes* expressing  
610 ovalbumin (LM-OVA) intravenously. LM-OVA was kindly provided by Prof. Audrey Gerard (Kennedy  
611 Institute of Rheumatology, University of Oxford). LM-OVA growth was done from frozen aliquots in Brain  
612 Heart Infusion (BHI) broth (Sigma, #53286-100G). Bacteria were used for infections when reaching  
613 exponential growth. Immune responses were tracked in the blood and at the memory phase spleens  
614 were harvested.

615 Immunofluorescence staining and confocal microscopy

616 At different timepoints post-stimulation (pre-mitotic or mitotic/post-mitotic), CD8<sup>+</sup> T cells were harvested.  
617 In some experiments, cells were incubated with 1-2  $\mu$ M MitoSOX™ Mitochondrial Superoxide Indicator  
618 (Invitrogen) for 15 min at 37°C prior to harvesting. Cells were washed in PBS and transferred on Poly-  
619 L-Lysine (Sigma-Aldrich) treated coverslips, followed by incubation for 45-60 min at 37 °C. Attached  
620 cells were fixed with 2% methanol-free paraformaldehyde (PFA) in PBS (ThermoScientific) for 10 min,  
621 permeabilized with 0.3% Triton X-100 (Sigma-Aldrich) for 10 min and blocked in PBS containing 2%  
622 bovine serum albumin (BSA, Sigma-Aldrich) and 0.01% Tween 20 (Sigma-Aldrich) for 1 h at room  
623 temperature. The following antibodies were used to perform immunofluorescence stainings in murine  
624 cells: mouse anti- $\beta$ -tubulin (Sigma-Aldrich), anti-mouse IgG AF488 (Abcam), anti-CD8 APC 53-6.7,  
625 BioLegend), anti-LC3B (D11) XP® Rabbit mAb PE (Cell Signalling). DAPI (Sigma-Aldrich) was used to  
626 detect DNA. ProLong™ Gold Antifade Mountant (ThermoScientific) was used as mounting medium.  
627 Mitotic cells (late anaphase to cytokinesis) were identified by nuclear morphology and/or presence of  
628 two microtubule organizing centres (MTOCs) and a clear tubulin bridge between two daughter cells.  
629 Forty to eighty Z-stacks (0.13 $\mu$ M) were acquired with a ZEISS 980 Airyscan 2 with a C-Apochromat  
630 63x/1.2 W Corr magnification objective and the ZenBlue software. Data were analyzed using  
631 Fiji/ImageJ. Thresholds for quantification were setup individually for each fluorophore. Asymmetry rates  
632 were calculated based on the integrated density (volume and fluorescence intensity measurements  
633 were considered) of cell cargoes inherited by each daughter cell. This was done by using the following  
634 calculation: (P1-P2)/(P1+P2), where P1 is the daughter cell with higher integrated density of CD8 or old  
635 mitochondria. Any values above 0.2 or below -0.2 were considered asymmetric, which corresponds to  
636 one daughter-cell inheriting at least 1.5 $\times$  more of a cell cargo than its sibling.

637 Planar Supported Lipid Bilayers (PSLB)

638 Planar supported lipid bilayers were made as described previously <sup>55</sup>. Briefly, glass coverslips were  
639 plasma-cleaned and assembled into disposable six-channel chambers (Ibidi). SLB were formed by  
640 incubation of each channel with small unilamellar vesicles containing 12.5 mol% 1,2-dioleoyl-sn-  
641 glycero-3-[(N-(5-amino-1-carboxypentyl) iminodiacetic acid) succinyl] (nickel salt) and 0.05 mol% 1,2-  
642 dioleoyl-sn-glycero-3-phosphoethanolamine-N-(cap biotinyl) (sodium salt) in 1,2-dioleoyl-sn-glycero-3-  
643 phosphocholine at total phospholipid concentration 0.4 mM. Chambers were filled with human serum  
644 albumin (HSA)-supplemented HEPES buffered saline (HBS), subsequently referred to as HBS/HSA.  
645 Following blocking with 5% casein in PBS containing 100  $\mu$ M NiSO<sub>4</sub>, to saturate NTA sites, fluorescently

646 labelled streptavidin was then coupled to biotin head groups. Biotinylated 2C11-fab fragments (30  
647 molecules/μm<sup>2</sup>) and His-tagged ICAM-1 (200 molecules/μm<sup>2</sup>), and CD80 (100 molecules/μm<sup>2</sup>) were  
648 then incubated with the bilayers at concentrations to achieve the indicated site densities. Bilayers were  
649 continuous liquid disordered phase as determined by fluorescence recovery after photobleaching with  
650 a 10 μm bleach spot on an FV1200 confocal microscope (Olympus).

651 T cell immunological synapse formation on PSLB

652 Naïve murine CD8<sup>+</sup> T cells were incubated at 37°C on SLB. After 10 min, cells were fixed with 4%  
653 methanol-free formaldehyde in PHEM buffer (10 mM EGTA, 2 mM MgCl<sub>2</sub>, 60 mM Pipes, 25 mM  
654 HEPES, pH 7.0) and permeabilized with 0.1% Triton X-100 for 20 min at RT. Anti-CD3 staining was  
655 used to identify TCR regions and actin was labelled with fluorescent phalloidin.

656 Total internal reflection fluorescence microscopy (TIRFM)

657 TIRFM was performed on an Olympus IX83 inverted microscope equipped with a 4-line (405 nm, 488  
658 nm, 561 nm, and 640 nm laser) illumination system. The system was fitted with an Olympus UApON  
659 150 × 1.45 numerical aperture objective, and a Photometrics Evolve Delta EMCCD camera to provide  
660 Nyquist sampling. Quantification of fluorescence intensity was performed with ImageJ.

661 Flow Cytometry

662 Blood samples used for kinetics analysis were obtained from the tail vein at weeks 1, 2 and 3 post-LM-  
663 OVA challenge. At end-timepoints, spleens were harvested and single-cell splenocytes were prepared  
664 by meshing whole spleens through 70 μm strainers using a 1 ml syringe plunger. When cytokine  
665 production was assessed, splenocytes were incubated at 37 °C for 1 h with 1 μM of SIINFEKL peptide,  
666 followed by 4 h in presence of SIINFEKL peptide + 10 μg/ml of brefeldin A (Sigma-Aldrich). Specific  
667 CD8<sup>+</sup> T cells were evaluated by incubation with SIINFEKL<sub>257-264</sub>-APC-Labeled or SIINFEKL<sub>257-264</sub>-  
668 BV421-Labeled tetramers (NIH Tetramer Core Facility at Emory University). Erythrocytes were lysed  
669 by Red Blood Cell (RBC) Lysis buffer (Invitrogen). Conjugated antibodies used for surface staining  
670 were: anti-CD127 A7R34, anti-CD25 PC61 (AF700, PE Cy7, Biolegend; APC, eBioscience), anti-CD44  
671 IM7 (AF700, BV785, PE, PerCPCy5.5, Biolegend), anti-CD45.1 A20 (BV785, FITC, PB, Biolegend),  
672 anti-CD45.2 104 (AF700, BV711, FITC, Biolegend), anti-CD62L MEL-14 (FITC, Biolegend; eF450,  
673 eBioscience), anti-KLRG1 2F1 (BV711, BV785, Biolegend), anti-CD8 53-6.7 (BV510, BV605, FITC, PE,  
674 Biolegend), anti-TCRβ H57-597 (APC-Cy7, PerCPCy5.5, Biolegend). Cells were incubated for 20 min  
675 at 4 °C. When intracellular staining was performed, cells were fixed/permed with 2× FACS Lysis Solution  
676 (BD Biosciences) with 0.08% Tween 20 (Sigma-Aldrich) for 10 min at RT, washed in PBS and incubated  
677 for 1 h at RT with anti-IL2 JES6-5H4 (APC, Biolegend), anti-IFNγ XMG1.2 (BV421, Biolegend) and anti-  
678 TNF MP6-XT22 (PE-Cy7, ThermoFischer). Identification of viable cells was done by fixable near-IR  
679 dead cell staining (Life Technologies). All samples were washed and stored in PBS containing 2% FBS  
680 (Sigma-Aldrich) and 5 mM of EDTA (Sigma-Aldrich) before acquisition. Stained samples were acquired  
681 on a FACS LSR II (R/B/V) or a Fortessa X20 (R/B/V/YG) flow cytometer (BD Biosciences) with  
682 FACSDiva software. Data analysis was done using FlowJo software (FlowJo Enterprise, version 10.10,  
683 BD Biosciences).

684 Cell sorting (FACS)

685 After activation, CTV- and SnapSubstrate-labelled MitoSnap CD8<sup>+</sup> T cells were harvested and stained  
686 for phenotypical markers (anti-CD44 IM7, anti-CD45.1 A20, anti-CD45.2 104, anti-CD8 53-6.7  
687 conjugated to different fluorophores depending on experiment, all Biolegend). Dead cells were excluded  
688 by staining cells with a fixable Live/Dead dye (Invitrogen, L34993 or L34957). Subpopulations of interest  
689 were sorted on a FACS Aria III cell sorter (BD Biosciences).

690 Metabolic reliance measured by protein translation

691 We used a modified version of the Scenith assay<sup>39</sup>, which describes a high correlation between protein  
692 translation and ATP production. New protein synthesis was measured using the Click-iT Plus OPP  
693 Protein Synthesis Assay (Thermo Fisher, C10456) according to manufacturer's protocol. In short, cells  
694 were incubated in T cell medium for 30 min at 37°C without any metabolic inhibitors or in presence of

695 1  $\mu$ M oligomycin (Merck), 100 mM 2DG (Merck), a combination of both or 1  $\mu$ M of SHIN1 (Cambridge  
696 Bioscience). This was followed by incubation with 10 $\mu$ M of alkynylated puromycin analog OPP for 30  
697 min at 37°C. Click Chemistry was performed with Alexa Fluor 488™ dye picolyl azide. Metabolic  
698 reliance was assessed by comparing the OPP gMFI, used as an indicator of the relative translation rate,  
699 of inhibited samples to the vehicle control.

700 Western Blot

701 Following (Z)-4-hydroxytamoxifen (Sigma-Aldrich, H7904-5MG) treatment for 24 h and/or baflomycin  
702 A1 (BafA) treatment (10 nM) for 2 h or not, cells were washed with PBS and lysed in RIPA lysis buffer  
703 (Sigma-Aldrich) supplemented with complete Protease Inhibitor Cocktail (Roche) and PhosSTOP  
704 (Roche). Protein concentration was calculated by using the BCA Assay (ThermoFisher). Samples were  
705 diluted in 4x Laemmli Sample Buffer (Bio-Rad) and boiled at 100 °C for 5 min. 20  $\mu$ g protein per sample  
706 were used for SDS-PAGE analysis. NuPAGE Novex 4%–12% Bis-Tris gradient gel (Invitrogen) with  
707 MOPS running buffer (Invitrogen) was used. Proteins were transferred to a PVDF membrane (Merck  
708 Millipore) and blocked with 5% skimmed milk-TBST (TBS 10x [Sigma-Aldrich] diluted to 1x in distilled  
709 water containing 0.1% Tween 20 [Sigma-Aldrich]) for 1h. Membranes were incubated at 4°C overnight  
710 with primary antibodies diluted in 1% skimmed milk-TBST and at room temperature for 1 h with  
711 secondary antibodies diluted in 1% skimmed milk-TBST supplemented 0.01% SDS. Primary antibodies  
712 used were: anti-ATG16L1, clone EPR15638 (Abcam, ab187671) and anti-GAPDH, clone 6C5 (Sigma-  
713 Aldrich, MAB374). Secondary antibodies used were: IRDye 680LT Goat anti-Mouse IgG (H + L) (Licor,  
714 926-680-70) and IRDye 800CW Goat anti-Rabbit IgG (H + L) (Licor, 926-322-11). Images were acquired  
715 using the Odyssey CLx Imaging System. Data were analyzed using Image Studio Lite or Fiji.

716 Mitochondrial isolation and flow cytometry (MitoFlow)

717 Autophagy-sufficient (*Atg16l1*<sup>fl/fl</sup> *Omp25*<sup>fl/fl</sup> *Ert2*<sup>Cre</sup>) and -deficient (*Atg16l1*<sup>fl/fl</sup> *Omp25*<sup>fl/fl</sup> *Ert2*<sup>Cre</sup>) MitoSnap  
718 CD8<sup>+</sup> T cells were activated, labelled for old (SNAP-Cell® TMR-Star, NEB) and young organelles  
719 (SNAP-Cell® Oregon Green, NEB), as previously described in the methods section, and after 40h  
720 washed with complete T cell medium. Cell pellets were resuspended in ice-cold mitochondria isolation  
721 buffer (320 mM sucrose, 2 mM EGTA, 10 mM Tris-HCl, at pH 7.2 in water) and homogenized with a  
722 Dounce homogenizer with a 2 ml reservoir capacity (Abcam). We performed 20 strokes with a type B  
723 pretzel. The homogenizer was rinsed with distilled water before each sample was processed to avoid  
724 cross-contamination. Differential centrifugation of homogenates was done at 1,000 xg (4 °C for 8 min),  
725 which resulted in a pellet containing whole cells and isolated nuclei first. The supernatant containing  
726 the mitochondria was then transferred into new tubes and centrifuged at 17,000 xg (4 °C for 15 min).  
727 Enriched mitochondria, which appeared as brown-colored pellets, were fixed in 1% PFA in 0.5 ml PBS  
728 on ice for 15 min, followed by a wash with PBS. Mitochondria were resuspended in blocking buffer  
729 containing anti-Tom20-BV421 antibody for 20 min at RT. After washing with PBS, mitochondria were  
730 resuspended in 250  $\mu$ l filtered (0.2  $\mu$ m) PBS and acquired using a BD Fortessa X-20 flow cytometer.  
731 The threshold for SSC-A (log-scale) was set to the minimum value (20,000) to allow acquisition of  
732 subcellular particles. Submicron Particle Size Reference Beads (0.5  $\mu$ m, 1  $\mu$ m and 2  $\mu$ m, Thermo Fisher  
733 Scientific) were also used to identify mitochondria.

734 Metabolic flux analysis

735 MitoSnap+ and MitoSnap- cells were purified by FACS and their oxygen consumption rates (OCR) were  
736 measured using a XF96 MitoStress Test (Seahorse Agilent, 103015-100). Activated CD8<sup>+</sup> T cells were  
737 washed in RPMI 1640 without sodium bicarbonate, 10 mM glucose, 1% FCS, 2 mM pyruvate and  
738 seeded in a XF plate (Agilent, 103793-100) coated with poly-L-lysine (Sigma-Aldrich) at equal densities  
739 in corresponding assay medium (XF Assay Medium, 103680-100) pH 7.4 supplemented with 10 mM  
740 glucose, 1 mM sodium pyruvate and 2 mM L-glutamine. Test compounds were sequentially injected to  
741 obtain the following concentrations: 1  $\mu$ M oligomycin, 1.5  $\mu$ M FCCP, 1  $\mu$ M rotenone and 1  $\mu$ M antimycin  
742 A. OCRs were normalized to cell number using CyQuant (Molecular Probes).

743 ATP synthesis assay

744 Sorted MitoSnap+ and MitoSnap- CD8<sup>+</sup> T cells were boiled in 100 mM Tris, 4 mM EDTA, pH 7.74 buffer  
745 for 2 min at 100°C. Following centrifugation, the supernatant was used for analysis. ATP levels were

746 assessed using the ATP Bioluminescence Assay Kit CLS II (Roche) following the manufacturer's  
747 instructions. The samples and ATP standard mixtures were swiftly combined with an equal volume of  
748 luciferase and promptly measured in a luminometer (BMG CLARIOstar Plus microplate reader).  
749 Normalization was performed by adjusting values based on the total number of sorted cells. Experiment  
750 was performed twice. Each experiment was done with 2 samples/group (each one pooled from 2  
751 biological replicates) and at least four technical replicates per group.

752 Proteomics

753 Proteomics analysis was done as previously described<sup>56</sup>. CD8<sup>hi</sup> and CD8<sup>lo</sup> or MitoSnap+ and MitoSnap-  
754 daughter-cells following naïve CD8<sup>+</sup> T cell activation were purified by FACS. Cell pellets were washed  
755 2x in PBS before being stored at -80°C prior to proteomics analysis. Samples were resuspended in 200  
756 µl of S-Trap lysis buffer (10% SDS, 100mM Triethylammonium bicarbonate) and sonicated for 15 min  
757 (30 s on, 30 s off, 100% Amplitude, 70% Pulse). Samples were centrifuged and supernatants were  
758 transferred to fresh tubes. Protein quantification was done using the Micro BCA Protein Assay Kit  
759 (ThermoFisher). 150 µg of protein was processed using S-Trap mini columns (Protifi, #CO2-mini-80).  
760 The samples were digested overnight with 3.75 µg of trypsin (ThermoFisher, Pierce Trypsin Protease  
761 MS-Grade, #90057) with a second digest with the same amount of trypsin for 6 h the following day.  
762 Peptides were extracted, dried under vacuum and resuspended to 50 µl with 1% Formic Acid  
763 (ThermoFisher, #85178) and quantified using the Pierce Quantitative Fluorometric Peptide Assay  
764 (ThermoFisher, #23290).

765 Peptides were injected onto a nanoscale C18 reverse-phase chromatography system (UltiMate 3000  
766 RSLC nano, ThermoFisher) and electrosprayed into an Orbitrap Exploris 480 Mass Spectrometer (MS)  
767 (ThermoFisher). For liquid chromatography the following buffers were used: buffer A (0.1% formic acid  
768 in Milli-Q water (v/v)) and buffer B (80% acetonitrile and 0.1% formic acid in Milli-Q water (v/v)). Samples  
769 were loaded at 10 µL/min onto a trap column (100 µm × 2 cm, PepMap nanoViper C18 column, 5 µm,  
770 100 Å, ThermoFisher) equilibrated in 0.1% trifluoroacetic acid (TFA). The trap column was washed for  
771 3 min at the same flow rate with 0.1% TFA then switched in-line with a ThermoFisher, resolving C18  
772 column (75 µm × 50 cm, PepMap RSLC C18 column, 2 µm, 100 Å). Peptides were eluted from the  
773 column at a constant flow rate of 300 nl/min with a linear gradient from 3% buffer B to 6% buffer B in 5  
774 min, then from 6% buffer B to 35% buffer B in 115 min, and finally from 35% buffer B to 80% buffer B  
775 within 7 min. The column was then washed with 80% buffer B for 4 min. Two blanks were run between  
776 each sample to reduce carry-over. The column was kept at a constant temperature of 50°C. The data  
777 was acquired using an easy spray source operated in positive mode with spray voltage at 2.60 kV, and  
778 the ion transfer tube temperature at 250°C. The MS was operated in DIA mode. A scan cycle comprised  
779 a full MS scan (m/z range from 350-1650), with RF lens at 40%, AGC target set to custom, normalised  
780 AGC target at 300%, maximum injection time mode set to custom, maximum injection time at 20 ms,  
781 microscan set to 1 and source fragmentation disabled. MS survey scan was followed by MS/MS DIA  
782 scan events using the following parameters: multiplex ions set to false, collision energy mode set to  
783 stepped, collision energy type set to normalized, HCD collision energies set to 25.5, 27 and 30%,  
784 orbitrap resolution 30000, first mass 200, RF lens 40%, AGC target set to custom, normalized AGC  
785 target 3000%, microscan set to 1 and maximum injection time 55 ms. Data for both MS scan and MS/MS  
786 DIA scan events were acquired in profile mode.

787 Analysis of the DIA data was carried out using Spectronaut Biognosys, AG (version 14.7.201007.47784  
788 for CD8<sup>hi</sup> and CD8<sup>lo</sup> cells obtained from young, *Atg16l1*-deficient and old mice; version  
789 17.6.230428.55965 for MitoSnap+ and MitoSnap- cells). Data was analysed using the direct DIA  
790 workflow, with the following settings: imputation, profiling and cross run normalization were disabled;  
791 data Filtering to Qvalue; Precursor Qvalue Cutoff and Protein Qvalue Cutoff (Experimental) set to 0.01;  
792 maximum of 2 missed trypsin cleavages; PSM, Protein and Peptide FDR levels set to 0.01; cysteine  
793 carbamidomethylation set as fixed modification and acetyl (N-term), deamidation (asparagine,  
794 glutamine), oxidation of methionine set as variable modifications. The database used for CD8<sup>hi</sup> and  
795 CD8<sup>lo</sup> cells was mouse\_swissprot\_isoforms\_extra\_trembl\_06\_20.fasta (2020-06) and for mitosnap  
796 samples was the *Mus musculus* proteome obtained from uniprot.org (2022-02). Data filtering, protein  
797 copy number and concentration quantification was performed in the Perseus software package, version  
798 1.6.6.0. Copy numbers were calculated using the proteomic ruler as described<sup>31</sup>. Samples were

799 grouped according to the condition. P values were calculated via a two-tailed, unequal-variance t-test  
800 on log-normalized data. Elements with P values < 0.05 were considered significant, with a fold-change  
801 cut-off > 1.5 or < 0.67.

802 **Single cell transcriptomics**

803 Single cell RNA sequencing libraries were prepared using the Chromium Single Cell 3' GEX v3.1 assay  
804 (10X Genomics). In short, cell suspensions were encapsulated into Gel Beads in Emulsion (GEMs)  
805 using the Chromium Controller. Within each GEM, cell lysis and barcoded reverse transcription of RNA  
806 occurred, followed by cDNA amplification. The amplified cDNA underwent library construction via  
807 fragmentation, end-repair, A-tailing, adaptor ligation, and index PCR. Final libraries were sequenced on  
808 an Illumina NovaSeq 6000 system. Initial data processing was conducted with Cell Ranger 7.2.0.

809 Filtered output matrices were processed using Seurat. After loading the data and assigning unique  
810 identifiers to each dataset, cells with more than 30% mitochondrial gene content were excluded to  
811 ensure data quality (we used a less strict threshold because we were also interested in mitochondrial  
812 gene expression). The datasets were normalized using SCTransform, and PCA was conducted for  
813 dimensionality reduction. Integration of the datasets was achieved using the Harmony algorithm,  
814 followed by clustering and differential expression analysis. Finally, the integrated data were visualized  
815 using UMAP (down sampled to 13,000 cells per group). This methodology enabled a robust analysis  
816 while accounting for technical variations and maintaining biological integrity.

817 **Statistical analysis**

818 To test if data point values were in a Gaussian distribution, a normality test was performed before  
819 applying parametric or non-parametric statistical analysis. When two groups were compared, unpaired  
820 Student's t test or Mann-Whitney test were applied. When comparisons were done across more than  
821 two experimental groups, analysis were performed using One-Way ANOVA or Two-Way ANOVA with  
822 post hoc Tukey's test multiple testing correction. P values were considered significant when < 0.05, and  
823 exact P values are provided in the figures. All analyses were done using GraphPad Prism 9 software.

824 **Data availability**

825 The datasets generated or analyzed in this study are available from the corresponding lead author on  
826 reasonable request.

827 **Acknowledgments**

828 We thank Dr. T. Youdale, Dr. L. Sinclair and Prof. D. Cantrell CBE, FRSE, FRS, FMedSci and the  
829 FingerPrints Proteomics Core Facility of the University of Dundee for their support with proteomics  
830 analysis. We thank T. Conrad, C. Fischer, C. Dietrich, F. Solinas and C. Braeuning from the BIH/MDC  
831 Genomics Platform for their support in generating the scRNASeq data. We thank E. Johnson (Dunn  
832 School, University of Oxford) for performing electron microscopy experiments. We thank P. C. Moreira,  
833 D. Andrew and M. Medghalchi (Kennedy Institute of Rheumatology BSU staff) for their support. We also  
834 thank L. Uhl for helping with LM-OVA infections. This work was funded by grants from the Wellcome  
835 Trust (Investigator award 103830/Z/14/Z and 220784/Z/20/Z to A.K.S., Sir Henry Wellcome Fellowship  
836 220452/Z/20/Z to M.B., and PhD studentship award 203803/Z/16/Z to F.C.R.), the Helmholtz association  
837 (Helmholtz Distinguished Professorship Funding to recruit top-level international female scientists (W3)  
838 to A.K.S.), the European Union's Horizon 2020 (Marie Skłodowska-Curie grant agreement number  
839 893676 to M.B. and ERC-2021-SyG\_951329 to E.C.B. and M.L.D.), the Swiss National Science  
840 Foundation (Early Postdoc.Mobility P2E2P3\_188074 to M.B.), the European Molecular Biology  
841 Organization (EMBO LT postdoctoral Fellowship - ALTF1155-2019 to A.V.L.V.) and the Kennedy Trust  
842 for Rheumatology Research (KTTR) to Y.F.Y. and M.L.D. Flow cytometry and microscopy facilities were  
843 supported by KTTR.

844 **Authors contributions**

845 M.B., A.V.L.V. and A.K.S., designed the experiments. M.B., A.V.L.V., E.B.C. and F.C.R. performed the  
846 experiments. H.B., M.L.D., P.K. provided expert assistance and guidance. M.B., A.V.L.V., A.H.K.  
847 analyzed the experiments. M.B. and A.K.S. wrote the manuscript.

848 **References**

- 849 1. Stemberger, C., Huster, K.M., Koffler, M., Anderl, F., Schiemann, M., Wagner, H., and Busch, D.H. (2007). A single naive CD8+ T cell precursor can develop into diverse effector and memory subsets. *Immunity* 27, 985-997. 10.1016/j.jimmuni.2007.10.012.
- 850 2. Gerlach, C., Rohr, J.C., Perie, L., van Rooij, N., van Heijst, J.W., Velds, A., Urbanus, J., Naik, S.H., Jacobs, H., Beltman, J.B., et al. (2013). Heterogeneous differentiation patterns of individual CD8+ T cells. *Science* 340, 635-639. 10.1126/science.1235487.
- 851 3. Moller, S.H., Hsueh, P.C., Yu, Y.R., Zhang, L., and Ho, P.C. (2022). Metabolic programs tailor T cell immunity in viral infection, cancer, and aging. *Cell Metab* 34, 378-395. 10.1016/j.cmet.2022.02.003.
- 852 4. Chang, J.T., Wherry, E.J., and Goldrath, A.W. (2014). Molecular regulation of effector and memory T cell differentiation. *Nat Immunol* 15, 1104-1115. 10.1038/ni.3031.
- 853 5. Henning, A.N., Roychoudhuri, R., and Restifo, N.P. (2018). Epigenetic control of CD8(+) T cell differentiation. *Nat Rev Immunol* 18, 340-356. 10.1038/nri.2017.146.
- 854 6. Alsaleh, G., Panse, I., Swadling, L., Zhang, H., Richter, F.C., Meyer, A., Lord, J., Barnes, E., Kleneman, P., Green, C., and Simon, A.K. (2020). Autophagy in T cells from aged donors is maintained by spermidine and correlates with function and vaccine responses. *Elife* 9. 10.7554/elife.57950.
- 855 7. Mittelbrunn, M., and Kroemer, G. (2021). Hallmarks of T cell aging. *Nat Immunol* 22, 687-698. 10.1038/s41590-021-00927-z.
- 856 8. Han, S., Georgiev, P., Ringel, A.E., Sharpe, A.H., and Haigis, M.C. (2023). Age-associated remodeling of T cell immunity and metabolism. *Cell Metab* 35, 36-55. 10.1016/j.cmet.2022.11.005.
- 857 9. Quinn, K.M., Fox, A., Harland, K.L., Russ, B.E., Li, J., Nguyen, T.H.O., Loh, L., Olshanksy, M., Naeem, H., Tsyanov, K., et al. (2018). Age-Related Decline in Primary CD8(+) T Cell Responses Is Associated with the Development of Senescence in Virtual Memory CD8(+) T Cells. *Cell Rep* 23, 3512-3524. 10.1016/j.celrep.2018.05.057.
- 858 10. Mogilenko, D.A., Shpynov, O., Andhey, P.S., Arthur, L., Swain, A., Esaulova, E., Brioschi, S., Shchukina, I., Kerndl, M., Bambouskova, M., et al. (2021). Comprehensive Profiling of an Aging Immune System Reveals Clonal GZMK(+) CD8(+) T Cells as Conserved Hallmark of Inflammaging. *Immunity* 54, 99-115 e112. 10.1016/j.jimmuni.2020.11.005.
- 859 11. Henson, S.M., Lanna, A., Riddell, N.E., Franzese, O., Macaulay, R., Griffiths, S.J., Puleston, D.J., Watson, A.S., Simon, A.K., Tooze, S.A., and Akbar, A.N. (2014). p38 signaling inhibits mTORC1-independent autophagy in senescent human CD8(+) T cells. *J Clin Invest* 124, 4004-4016. 10.1172/JCI75051.
- 860 12. Borsig, M., Barandun, N., Grabnitz, F., Barnstorf, I., Baumann, N.S., Pallmer, K., Baumann, S., Stark, D., Balaz, M., Oetiker, N., et al. (2021). Asymmetric cell division shapes naive and virtual memory T-cell immunity during ageing. *Nat Commun* 12, 2715. 10.1038/s41467-021-22954-y.
- 861 13. Sturmlechner, I., Jain, A., Mu, Y., Weyand, C.M., and Goronzy, J.J. (2023). T cell fate decisions during memory cell generation with aging. *Semin Immunol* 69, 101800. 10.1016/j.smim.2023.101800.
- 862 14. Clarke, A.J., and Simon, A.K. (2019). Autophagy in the renewal, differentiation and homeostasis of immune cells. *Nat Rev Immunol* 19, 170-183. 10.1038/s41577-018-0095-2.
- 863 15. Puleston, D.J., Zhang, H., Powell, T.J., Lipina, E., Sims, S., Panse, I., Watson, A.S., Cerundolo, V., Townsend, A.R., Kleneman, P., and Simon, A.K. (2014). Autophagy is a critical regulator of memory CD8(+) T cell formation. *Elife* 3. 10.7554/elife.03706.
- 864 16. Xu, X., Araki, K., Li, S., Han, J.H., Ye, L., Tan, W.G., Konieczny, B.T., Bruinsma, M.W., Martinez, J., Pearce, E.L., et al. (2014). Autophagy is essential for effector CD8(+) T cell survival and memory formation. *Nat Immunol* 15, 1152-1161. 10.1038/ni.3025.

897 17. Franco, F., Bevilacqua, A., Wu, R.M., Kao, K.C., Lin, C.P., Rousseau, L., Peng, F.T., Chuang, 898 Y.M., Peng, J.J., Park, J., et al. (2023). Regulatory circuits of mitophagy restrict distinct modes 899 of cell death during memory CD8(+) T cell formation. *Sci Immunol* 8, eadf7579. 900 10.1126/sciimmunol.adf7579.

901 18. Pua, H.H., Guo, J., Komatsu, M., and He, Y.W. (2009). Autophagy is essential for mitochondrial 902 clearance in mature T lymphocytes. *J Immunol* 182, 4046-4055. 10.4049/jimmunol.0801143.

903 19. Sunchu, B., and Cabernard, C. (2020). Principles and mechanisms of asymmetric cell division. 904 *Development* 147. 10.1242/dev.167650.

905 20. Cobbold, S.P., Adams, E., Howie, D., and Waldmann, H. (2018). CD4(+) T Cell Fate Decisions 906 Are Stochastic, Precede Cell Division, Depend on GITR Co-Stimulation, and Are Associated 907 With Uropodium Development. *Front Immunol* 9, 1381. 10.3389/fimmu.2018.01381.

908 21. Chang, J.T., Palanivel, V.R., Kinjyo, I., Schambach, F., Intlekofer, A.M., Banerjee, A., 909 Longworth, S.A., Vinup, K.E., Mrass, P., Oliaro, J., et al. (2007). Asymmetric T lymphocyte 910 division in the initiation of adaptive immune responses. *Science* 315, 1687-1691. 911 10.1126/science.1139393.

912 22. Grabnitz, F., Stark, D., Shlesinger, D., Petkidis, A., Borsig, M., Yermanos, A., Carr, A., 913 Barandun, N., Wehling, A., Balaz, M., et al. (2023). Asymmetric cell division safeguards 914 memory CD8 T cell development. *Cell Rep* 42, 112468. 10.1016/j.celrep.2023.112468.

915 23. King, C.G., Koehli, S., Hausmann, B., Schmaler, M., Zehn, D., and Palmer, E. (2012). T cell 916 affinity regulates asymmetric division, effector cell differentiation, and tissue pathology. 917 *Immunity* 37, 709-720. 10.1016/j.jimmuni.2012.06.021.

918 24. Chang, J.T., Ciocca, M.L., Kinjyo, I., Palanivel, V.R., McClurkin, C.E., DeJong, C.S., Mooney, 919 E.C., Kim, J.S., Steinel, N.C., Oliaro, J., et al. (2011). Asymmetric proteasome segregation as 920 a mechanism for unequal partitioning of the transcription factor T-bet during T lymphocyte 921 division. *Immunity* 34, 492-504. 10.1016/j.jimmuni.2011.03.017.

922 25. Polizzi, K.N., Sun, I.H., Patel, C.H., Lo, Y.C., Oh, M.H., Waickman, A.T., Tam, A.J., Blosser, 923 R.L., Wen, J., Delgoffe, G.M., and Powell, J.D. (2016). Asymmetric inheritance of mTORC1 924 kinase activity during division dictates CD8(+) T cell differentiation. *Nat Immunol* 17, 704-711. 925 10.1038/ni.3438.

926 26. Verbist, K.C., Guy, C.S., Milasta, S., Liedmann, S., Kaminski, M.M., Wang, R., and Green, D.R. 927 (2016). Metabolic maintenance of cell asymmetry following division in activated T lymphocytes. 928 *Nature* 532, 389-393. 10.1038/nature17442.

929 27. Liedmann, S., Liu, X., Guy, C.S., Crawford, J.C., Rodriguez, D.A., Kuzuoglu-Ozturk, D., Guo, 930 A., Verbist, K.C., Temirov, J., Chen, M.J., et al. (2022). Localization of a TORC1-eIF4F 931 translation complex during CD8(+) T cell activation drives divergent cell fate. *Mol Cell* 82, 2401- 932 2414 e2409. 10.1016/j.molcel.2022.04.016.

933 28. Borsig, M., Barnstorff, I., Baumann, N.S., Palmer, K., Yermanos, A., Grabnitz, F., Barandun, N., 934 Hausmann, A., Sandu, I., Barral, Y., and Oxenius, A. (2019). Modulation of asymmetric cell 935 division as a mechanism to boost CD8(+) T cell memory. *Sci Immunol* 4. 936 10.1126/sciimmunol.aav1730.

937 29. Metz, P.J., Arsenio, J., Kakaradov, B., Kim, S.H., Remedios, K.A., Oakley, K., Akimoto, K., 938 Ohno, S., Yeo, G.W., and Chang, J.T. (2015). Regulation of asymmetric division and CD8+ T 939 lymphocyte fate specification by protein kinase Czeta and protein kinase Clambda/ iota. *J Immunol* 194, 2249-2259. 10.4049/jimmunol.1401652.

941 30. Quezada, L.K., Jin, W., Liu, Y.C., Kim, E.S., He, Z., Indralingam, C.S., Tysl, T., Labarta-Bajo, 942 L., Wehrens, E.J., Jo, Y., et al. (2023). Early transcriptional and epigenetic divergence of CD8+ 943 T cells responding to acute versus chronic infection. *PLoS Biol* 21, e3001983. 944 10.1371/journal.pbio.3001983.

945 31. Wisniewski, J.R., Hein, M.Y., Cox, J., and Mann, M. (2014). A "proteomic ruler" for protein copy  
946 number and concentration estimation without spike-in standards. *Mol Cell Proteomics* 13, 3497-  
947 3506. 10.1074/mcp.M113.037309.

948 32. Buck, M.D., O'Sullivan, D., Klein Geltink, R.I., Curtis, J.D., Chang, C.H., Sanin, D.E., Qiu, J.,  
949 Kretz, O., Braas, D., van der Windt, G.J., et al. (2016). Mitochondrial Dynamics Controls T Cell  
950 Fate through Metabolic Programming. *Cell* 166, 63-76. 10.1016/j.cell.2016.05.035.

951 33. Pearce, E.L., Walsh, M.C., Cejas, P.J., Harms, G.M., Shen, H., Wang, L.S., Jones, R.G., and  
952 Choi, Y. (2009). Enhancing CD8 T-cell memory by modulating fatty acid metabolism. *Nature*  
953 460, 103-107. 10.1038/nature08097.

954 34. Emurla, H., Barral, Y., and Oxenius, A. (2021). Role of mitotic diffusion barriers in regulating  
955 the asymmetric division of activated CD8 T cells. *bioRxiv*, 2021.2009.2010.458880.  
956 10.1101/2021.09.10.458880.

957 35. Keppler, A., Gendreizig, S., Gronemeyer, T., Pick, H., Vogel, H., and Johnsson, K. (2003). A  
958 general method for the covalent labeling of fusion proteins with small molecules in vivo. *Nat  
959 Biotechnol* 21, 86-89. 10.1038/nbt765.

960 36. Katajisto, P., Dohla, J., Chaffer, C.L., Pentinmikko, N., Marjanovic, N., Iqbal, S., Zoncu, R.,  
961 Chen, W., Weinberg, R.A., and Sabatini, D.M. (2015). Stem cells. Asymmetric apportioning of  
962 aged mitochondria between daughter cells is required for stemness. *Science* 348, 340-343.  
963 10.1126/science.1260384.

964 37. Hogquist, K.A., Jameson, S.C., Heath, W.R., Howard, J.L., Bevan, M.J., and Carbone, F.R.  
965 (1994). T cell receptor antagonist peptides induce positive selection. *Cell* 76, 17-27.  
966 10.1016/0092-8674(94)90169-4.

967 38. Plambeck, M., Kazeroonian, A., Loeffler, D., Kretschmer, L., Salinno, C., Schroeder, T., Busch,  
968 D.H., Flossdorf, M., and Buchholz, V.R. (2022). Heritable changes in division speed accompany  
969 the diversification of single T cell fate. *Proc Natl Acad Sci U S A* 119.  
970 10.1073/pnas.2116260119.

971 39. Arguello, R.J., Combes, A.J., Char, R., Gigan, J.P., Baaziz, A.I., Bousiquot, E., Camosseto, V.,  
972 Samad, B., Tsui, J., Yan, P., et al. (2020). SCENITH: A Flow Cytometry-Based Method to  
973 Functionally Profile Energy Metabolism with Single-Cell Resolution. *Cell Metab* 32, 1063-1075  
974 e1067. 10.1016/j.cmet.2020.11.007.

975 40. Jia, W., He, M.X., McLeod, I.X., Guo, J., Ji, D., and He, Y.W. (2015). Autophagy regulates T  
976 lymphocyte proliferation through selective degradation of the cell-cycle inhibitor  
977 CDKN1B/p27Kip1. *Autophagy* 11, 2335-2345. 10.1080/15548627.2015.1110666.

978 41. Pichierri, P., Ammazzalorso, F., Bignami, M., and Franchitto, A. (2011). The Werner syndrome  
979 protein: linking the replication checkpoint response to genome stability. *Aging (Albany NY)* 3,  
980 311-318. 10.18632/aging.100293.

981 42. Araki, K., Turner, A.P., Shaffer, V.O., Gangappa, S., Keller, S.A., Bachmann, M.F., Larsen,  
982 C.P., and Ahmed, R. (2009). mTOR regulates memory CD8 T-cell differentiation. *Nature* 460,  
983 108-112. 10.1038/nature08155.

984 43. Polizzi, K.N., Patel, C.H., Sun, I.H., Oh, M.H., Waickman, A.T., Wen, J., Delgoffe, G.M., and  
985 Powell, J.D. (2015). mTORC1 and mTORC2 selectively regulate CD8(+) T cell differentiation.  
986 *J Clin Invest* 125, 2090-2108. 10.1172/JCI77746.

987 44. Kakaradov, B., Arsenio, J., Widjaja, C.E., He, Z., Aigner, S., Metz, P.J., Yu, B., Wehrens, E.J.,  
988 Lopez, J., Kim, S.H., et al. (2017). Early transcriptional and epigenetic regulation of CD8(+) T  
989 cell differentiation revealed by single-cell RNA sequencing. *Nat Immunol* 18, 422-432.  
990 10.1038/ni.3688.

991 45. Sugiura, A., Andrejeva, G., Voss, K., Heintzman, D.R., Xu, X., Madden, M.Z., Ye, X., Beier,  
992 K.L., Chowdhury, N.U., Wolf, M.M., et al. (2022). MTHFD2 is a metabolic checkpoint controlling  
993 effector and regulatory T cell fate and function. *Immunity* 55, 65-81 e69.  
994 10.1016/j.immuni.2021.10.011.

995 46. Franco, F., Jaccard, A., Romero, P., Yu, Y.R., and Ho, P.C. (2020). Metabolic and epigenetic  
996 regulation of T-cell exhaustion. *Nat Metab* 2, 1001-1012. 10.1038/s42255-020-00280-9.

997 47. van der Windt, G.J., Everts, B., Chang, C.H., Curtis, J.D., Freitas, T.C., Amiel, E., Pearce, E.J.,  
998 and Pearce, E.L. (2012). Mitochondrial respiratory capacity is a critical regulator of CD8+ T cell  
999 memory development. *Immunity* 36, 68-78. 10.1016/j.jimmuni.2011.12.007.

1000 48. O'Sullivan, D., van der Windt, G.J., Huang, S.C., Curtis, J.D., Chang, C.H., Buck, M.D., Qiu, J.,  
1001 Smith, A.M., Lam, W.Y., DiPlato, L.M., et al. (2014). Memory CD8(+) T cells use cell-intrinsic  
1002 lipolysis to support the metabolic programming necessary for development. *Immunity* 41, 75-  
1003 88. 10.1016/j.jimmuni.2014.06.005.

1004 49. Corrado, M., Samardzic, D., Giacomello, M., Rana, N., Pearce, E.L., and Scorrano, L. (2021).  
1005 Deletion of the mitochondria-shaping protein Opa1 during early thymocyte maturation impacts  
1006 mature memory T cell metabolism. *Cell Death Differ* 28, 2194-2206. 10.1038/s41418-021-  
1007 00747-6.

1008 50. Girotra, M., Chiang, Y.H., Charmoy, M., Ginefra, P., Hope, H.C., Bataclan, C., Yu, Y.R., Schyrr,  
1009 F., Franco, F., Geiger, H., et al. (2023). Induction of mitochondrial recycling reverts age-  
1010 associated decline of the hematopoietic and immune systems. *Nat Aging* 3, 1057-1066.  
1011 10.1038/s43587-023-00473-3.

1012 51. Endow, S.A., Kull, F.J., and Liu, H. (2010). Kinesins at a glance. *J Cell Sci* 123, 3420-3424.  
1013 10.1242/jcs.064113.

1014 52. Ducker, G.S., and Rabinowitz, J.D. (2017). One-Carbon Metabolism in Health and Disease.  
1015 *Cell Metab* 25, 27-42. 10.1016/j.cmet.2016.08.009.

1016 53. Ma, E.H., Bantug, G., Griss, T., Condotta, S., Johnson, R.M., Samborska, B., Mainolfi, N., Suri,  
1017 V., Guak, H., Balmer, M.L., et al. (2017). Serine Is an Essential Metabolite for Effector T Cell  
1018 Expansion. *Cell Metab* 25, 345-357. 10.1016/j.cmet.2016.12.011.

1019 54. Loeffler, D., Schneiter, F., Wang, W., Wehling, A., Kull, T., Lengerke, C., Manz, M.G., and  
1020 Schroeder, T. (2022). Asymmetric organelle inheritance predicts human blood stem cell fate.  
1021 *Blood* 139, 2011-2023. 10.1182/blood.2020009778.

1022 55. Alpert, A., Pickman, Y., Leipold, M., Rosenberg-Hasson, Y., Ji, X., Gaujoux, R., Rabani, H.,  
1023 Starosvetsky, E., Kveler, K., Schaffert, S., et al. (2019). A clinically meaningful metric of immune  
1024 age derived from high-dimensional longitudinal monitoring. *Nat Med* 25, 487-495.  
1025 10.1038/s41591-019-0381-y.

1026 56. Jenkins, B.J., Blagih, J., Ponce-Garcia, F.M., Canavan, M., Gudgeon, N., Eastham, S., Hill, D.,  
1027 Hanlon, M.M., Ma, E.H., Bishop, E.L., et al. (2023). Canagliflozin impairs T cell effector function  
1028 via metabolic suppression in autoimmunity. *Cell Metab* 35, 1132-1146 e1139.  
1029 10.1016/j.cmet.2023.05.001.

1030